ASSESSMENT OF THE FINGERPRINTING METHOD FOR SPENT FUEL VERIFICATION IN MACSTOR KN-400 CANDU DRY STORAGE

A Thesis

by

NANDAN GOWTHAHALLI CHANDREGOWDA

Submitted to the Office of Graduate Studies of
Texas A&M University
in partial fulfillment of the requirements for the degree of

MASTER OF SCIENCE

August 2012

Major Subject: Nuclear Engineering

ASSESSMENT OF THE FINGERPRINTING METHOD FOR SPENT FUEL VERIFICATION IN MACSTOR KN-400 CANDU DRY STORAGE

A Thesis

by

NANDAN GOWTHAHALLI CHANDREGOWDA

Submitted to the Office of Graduate Studies of
Texas A&M University
in partial fulfillment of the requirements for the degree of

MASTER OF SCIENCE

Approved by:

Co-Chairs of Committee,	William S. Charlton
	Sunil S. Chirayath
Committee Members,	Craig M. Marianno
	Sunil P. Khatri
Head of Department,	Yassin A. Hassan

August 2012

Major Subject: Nuclear Engineering

ABSTRACT

Assessment of the Fingerprinting Method for Spent Fuel Verification in MACSTOR KN-400 CANDU Dry Storage. (August 2012)

Nandan Gowthahalli Chandregowda, B.S; M.S., Mangalore University, India

Co-Chairs of Advisory Committee: Dr. William S. Charlton
Dr. Sunil S. Chirayath

The Korea Hydro and Nuclear Power has built a new modular type of dry storage facility, known as MACSTOR KN-400 at Wolsong reactor site. The building has the capacity to store up to 24000 CANDU spent fuel bundles in a 4 rows by 10 columns arrangement of silos. The MACSTOR KN-400 consists of 40 silos; each silo has 10 storage baskets, each of which can store 60 CANDU spent fuel bundles.

The development of an effective method for spent fuel verification at the MACSTOR KN-400 storage facility is necessary in order for the International Atomic Energy Agency (IAEA) to meet with safeguards regulations. The IAEA is interested in having a new effective method of re-verification of the nuclear material in the MACSTOR KN-400 dry storage facility in the event of any loss of continuity of knowledge, which occasionally happens when the installed seals fail.

In the thesis work, MCNP models of central and corner structures of the MACSTOR KN-400 facility are developed, since both have different types of re-verification system. Both gamma and neutron simulations were carried out using the MCNP models developed for MACSTOR KN-400. The CANDU spent fuel bundle with

discharge burnup of 7.5 GWD/t (burned at specific power of 28.39 MW/t) and 10 years cooled was considered for radiation source term estimation.

For both the structures, MCNP simulations of gamma transport were done by including Cadmium-Zinc-Telluride (CZT) detector inside the re-verification tube. Gamma analyses for different spent fuel bundle diversion scenarios were carried out. It was observed that for diversion scenarios wherein the bundles are removed from the inner portions of the basket (opposite side of the collimator of the re-verification tube), it was difficult to conclude whether diversion has taken place based on the change in gamma radiation signals. Similar MCNP simulations of neutron transport were carried out by integrating helium-3 detector inside the re-verification tube and the results obtained for various diversion scenarios were encouraging and can be used to detect some spent fuel diversion cases. In the central structure, it was observed that addition of moderating material between the spent fuel and the detector increased the sensitivity of the detecting system for various diversion cases for neutron simulations.

In the worst scenario, the diverting state could divert 14 spent fuel bundles from each of 10 baskets in a silo from the basket region opposite to the collimator of the re-verification tube. The non-detection probability for this scenario is close to 1. This diversion cannot be easily detected using the currently designed detection system. In order to increase the detection probability, either the design of the facility must be changed or other safeguard methods, such as containment and surveillance methods must be used for safeguarding the nuclear material at the facility.

ACKNOWLEDGEMENTS

I would like to take this opportunity to thank my advisor Dr. William S. Charlton for the opportunity he provided for me to work on this project. His guidance and advices are really precious. I would also like to thank Dr. Sunil S. Chirayath for his kind hearted support and care. His guidance and advices are the strength behind the completion of this work. There is a lot to learn from Dr. Charlton and Dr. Chirayath. I would also like to acknowledge Dr. Paul Nelson for helping me to start graduate school at Texas A&M University and to overcome all the difficulties associated with coming from India to the United States of America. I would also like to thank my committee members Dr. Craig M. Marianno and Dr. Sunil P. Khatri for their support and valuable advice. I would also like to thank Dr. Young Ham and Dr. Shiva Sitaraman, Lawrence Livermore National Laboratory (LLNL) for sponsoring the project and for their co-operation and valuable guidance.

This is one of the best opportunities for me to thank my dearest friend Ms. Joe Justina (Bataanii) for her continued support. She is one of the real strengths in my life. My lovely parents, Mr. Chandregowda and Mrs. Sumitra, my sister Ms. Navyashree, my brother Mr. Naveen GC, and my sister in law Mrs. Bindu Naveen, who always believed in me and supported me all through my life, deserve a hearty thanks and appreciation. I also like to thank my life-partner Ms. Ramya BC for being patient and being with me during my bad days. I would also take this opportunity to thank all my family members and friends for being with me and supporting me.

TABLE OF CONTENTS

CHAPTER Page

Page

LIST OF FIGURES

FIGURE Page

FIGURE Page

FIGURE Page

LIST OF TABLES

TABLE Page

CHAPTER I

INTRODUCTION

I.A. Motivation and Objectives

The Republic of Korea currently has four CANDU reactors at Wolsong reactor site. At the reactor site, spent fuel bundles discharged from the reactors are transferred to an interim dry storage facility after cooling in a spent fuel pool for several years. As the Wolsong reactor site does not have enough space for further extension of its existing interim dry storage facility, the Korea Hydro and Nuclear Power has built a new modular type of dry storage facility, known as MACSTOR KN-400[1], shown in Fig. 1. The MACSTOR KN-400 module is based on the MACSTOR-200 design[2] but has twice the storage capacity. The building has the capacity to store up to 24000 CANDU spent fuel bundles in a 4 rows by 10 columns arrangement of silos. Each silo has 10 storage baskets and each basket can store 60 CANDU spent fuel bundles.

The MACSTOR KN-400 has four re-verification tubes in the center and 24 re-verification tubes at the periphery to verify the presence of stored spent fuel bundles. A fingerprinting method for re-verification of stored spent fuel bundles has not been fully assessed for this new MACSTOR KN-400 type of spent fuel dry storage facility. Development of effective methods for spent fuel verification at the MACSTOR KN-400 storage facility is necessary in order for the International Atomic Energy Agency

---

This thesis follows the style of *Nuclear Technology*.

(IAEA) to assess the compliance with safeguards regulations. The IAEA is interested in having a new effective spent fuel re-verification method in the dry storage facility in the event of any loss of continuity of knowledge (COK), which occasionally happens when the seals installed fail.

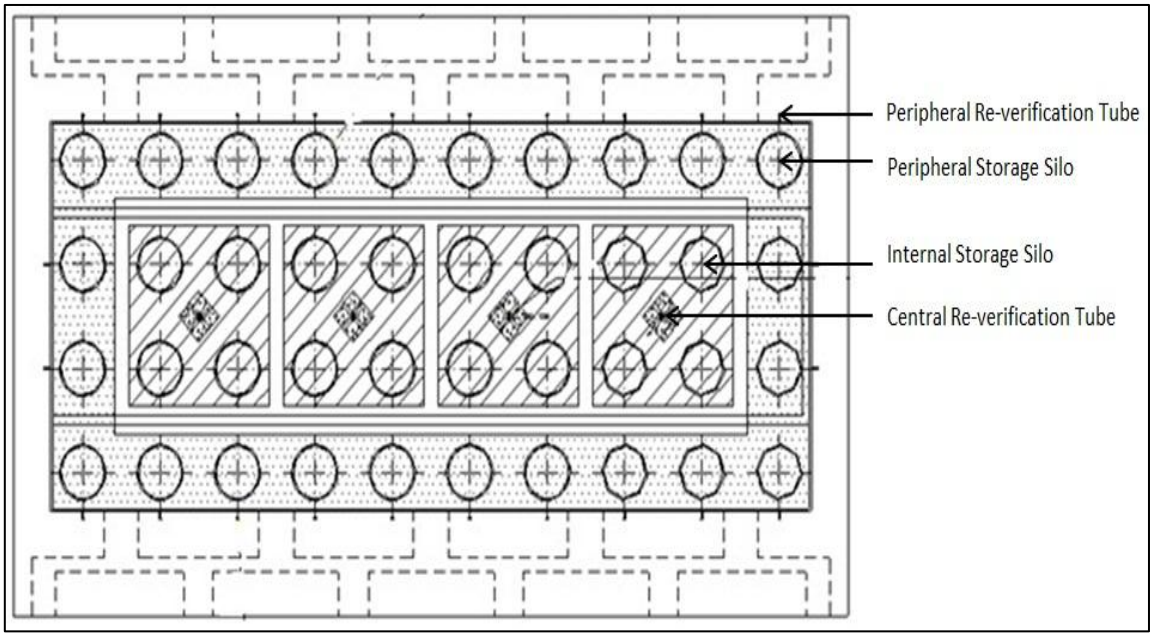

Fig. 1: Plan view of MACSTOR KN-400 CANDU spent fuel dry storage.

The objective of this thesis was to evaluate the gamma and neutron radiation fingerprinting method for spent fuel verification in MACSTOR KN-400 CANDU dry storage facility. The study included:

(1) Estimation of gamma and neutron radiation source terms of CANDU reactor spent fuel using SCALE6 (ORIGEN-ARP)[3],

(2) Modeling of the MACSTOR KN-400 geometry structure to perform gamma and neutron radiation transport simulations using Monte Carlo code MCNP[4] to arrive at gamma and neutron signals at the detectors inside the re-verification tube, and

(3) Sensitivity to the various spent fuel bundle diversion scenarios.

Based on results of the simulations, an estimate of non-detection probability will be made for diverting one significant quantity (SQ) of plutonium and uranium, significant quantity being 8 kg for plutonium and 20 t for depleted uranium.

Brief explanation of CANDU reactor and its fuel characteristics is made in the following paragraph for better understanding of the thesis subject matter.

I.B. CANDU Reactor and Fuel

The CANada Deuterium-Uranium (CANDU) reactor under study is a Canadian designed pressurized heavy water nuclear reactor which uses natural uranium as fuel, heavy water as moderator, heavy water as primary coolant, and light water as secondary coolant. It has an installed capacity 700 MWe[5]. The CANDU fuel is made out of natural uranium in the form of uranium dioxide (UO_2). The fuel pellets with size 1.54 cm (height) × 1.215 cm (diameter) are made of UO_2, encased in a zircaloy-4 cladding to form fuel pins. A typical CANDU fuel pin contains 31 fuel pellets. These fuel pins are bundled together with the help of end plates to form a CANDU fuel bundle. There are about 5 CANDU fuel bundle designs. The CANDU reactors at Wolsung reactor site use the Bruce 37-element design. The Bruce 37-element design CANDU fuel bundle is 49.53 cm long and has 10.25 cm diameter[6]. Whole fuel bundle weighs about 24 kg and

in that 19.2 kg in natural uranium. The structure of a CANDU fuel bundle along with a reactor vessel is shown in Fig. 2.

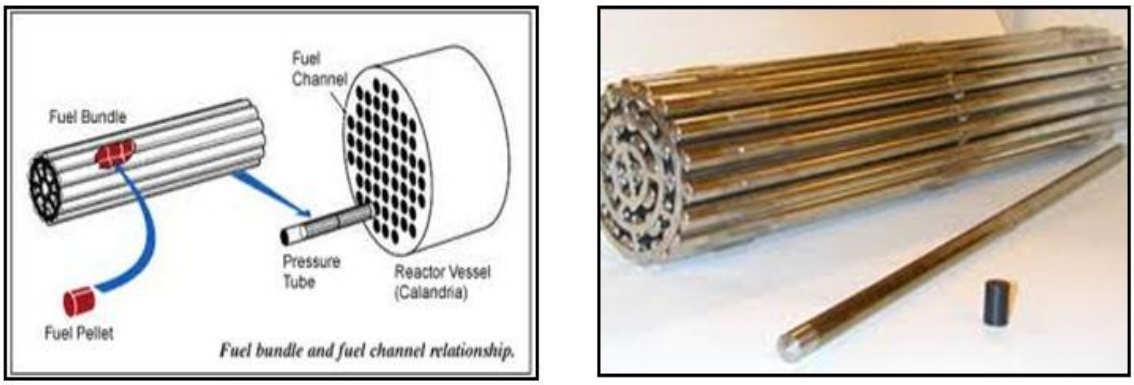

Fig. 2. Structure of a CANDU fuel bundle

Typically, one fuel channel of the reactor will be refueled per day and eight of the twelve fuel bundles in a fuel channel are replaced during a refueling operation. After the irradiation of fuel in the reactor for about 12-24 months, nuclear fuel is removed from the reactor because of the reduction in fissile content as well as the build-up of fission products and transuranics that absorbs neutrons. When removed from the reactor, a fuel bundle will emit gamma and neutron radiation (principally from the fission products) along with heat. Reactor discharged fuel is unloaded into a spent fuel storage pool immediately adjacent to the reactor to allow the radiation levels to decrease. In the pool, the water shields the radiation and absorbs the heat. Spent fuel is cooled in the pool for 5-10 years before moving into a dry storage facility cooled by air. However, both kinds of storage are intended only as an interim step before the spent fuel is either reprocessed

or sent to final disposal. The longer the spent fuel is stored, the easier it is to handle, due to the decay of radioactivity and decrease in heat emission.

I.C. Types of Dry Storage Facility for Spent Fuel

There are different types of dry storage systems for spent fuel, namely: casks, silos, vault facilities (CANSTOR, MACSTOR 200, MACSTOR KN-400, etc.)[7]. Dry storage systems for spent fuel generally remove decay heat by passive cooling with air and will have steel or concrete as the radiation barrier. They also provide the advantage of incremental storage capacity expansion by allowing additional storage capacity to be constructed on a need basis, and have low operating costs. Spent fuel from the reactor must be stored in water pools for about five years to make it possible to store it in a dry storage facility.

I.C.1 Casks

In a cask system, a flat bed of concrete is provided, and large casks that contain spent fuel can be added as needed to store the spent fuel. The casks provide both shielding and containment. The spent fuel in the casks is passively cooled by air. Originally, casks were designed only for spent fuel storage, but recently, some casks designs have been developed for both storage and transport (dual purpose) of spent fuel. Fig. 3 shows typical dry spent fuel storage casks at a nuclear power plant in the United States[7].

I.C.2 Silos

In a silo storage system, the spent fuel is stored in concrete cylinders, either vertical or horizontal. Concrete cylinders are fitted with metal inner liners or separate metal canisters, concrete provides the radiation shielding while the sealed inner metal liner or canister provides containment. Spent fuel is cooled in the pools before storing in the silos. The spent fuel in silos is passively cooled by air.

Fig. 3. Concrete casks at a U.S. nuclear power plant

I.C.3 Dry Storage Vaults

Vaults consist of reinforced concrete buildings containing arrays of storage cavities suitable for containment of spent fuel units. The exterior concrete structure of the vault

serves as the radiation barrier. The fuel is typically stored in sealed metal storage tubes or storage cylinders, which may hold one or several fuel assemblies; these provide containment of the radioactive material in the spent fuel. Heat from the spent fuel assembly is removed in vault systems by either forced or natural air convection. The advantage of a vault system is that for storage of very large quantities of spent fuel at a single facility, the cost of vaults are comparatively lower than the cost of other type of storage system.

I.C.4 MACSTOR (Modular Air Cooled STORage) KN-400

The MACSTOR KN-400 is a vault type of storage facility, which is based on MACSTOR-200[2] (which is already in use at Gentilly Nuclear Generating Station, Canada[8]) module design, (shown earlier in Fig. 1), but has twice the capacity and twice the number of storage silos. The MACSTOR KN-400 facility contains 40 dry fuel storage silos, each of which houses 10 spent fuel baskets. The 40 storage silos are arranged in a 4 rows by 10 columns (refer Fig. 1), with 24 located close to periphery walls of the module and 16 located internally.

I.D. Problems Associated with Spent Fuel Re-verification in MACSTOR KN-400

The MACSTOR KN-400 is a new type of CANDU spent fuel dry storage system for which an effective safeguard system needs to be developed. Re-verification is an IAEA safeguard requirement to ensure that the stored nuclear material in the facility is not diverted for undeclared purpose or activity by the state or organization. This is required

to monitor the presence of spent fuel in the storage silos by measuring the gamma and neutron signals of each irradiated fuel storage basket once the storage silos are loaded with spent fuel bundles. To achieve this on the existing MACSTOR-200 design, a re-verification tube, running inside the module walls, is provided for each storage silo. The gamma or neutron profile is read by lowering a detector inside the tube so that the respective spectrum can be registered at the level of each basket. For the 24 peripheral storage silos, this method of measurement is retained on the MACSTOR KN-400 module[2]. However, an alternate method is required for the 16 internal dry fuel storage silos since they are located some distance from the module walls. In an attempt to solve this problem, central re-verification tubes were added to MACSTOR KN-400 (Refer Fig. 1), which also facilitates the measurement of the gamma or neutron signal of fuel baskets in the surrounding 16 storage silos. The shielding portion of each column consists of a central hollow steel column surrounded by a square concrete column. The carbon steel re-verification tube is housed inside the central metal column.

In order to maximize the signal from specific fuel basket, the square columns are provided with viewing tubes, called collimators, which are used to increase the signal from the storage basket being measured. The collimators are arranged in a spiral manner along the height of the column, each one having a viewing angle towards the position of a specific fuel storage basket[9] as shown in Fig. 4. The collimators provide an unshielded path from the targeted fuel storage basket to the inner re-verification tube. The gamma or neutron profile is read by lowering a detector inside the re-verification tube so that the signal can be registered at the level of each basket. The arrangement of background

shielding and direct reading via the collimators helps to maximize the radiation signal from each viewed basket while minimizing background radiation originating from the surrounding fuel storage baskets.

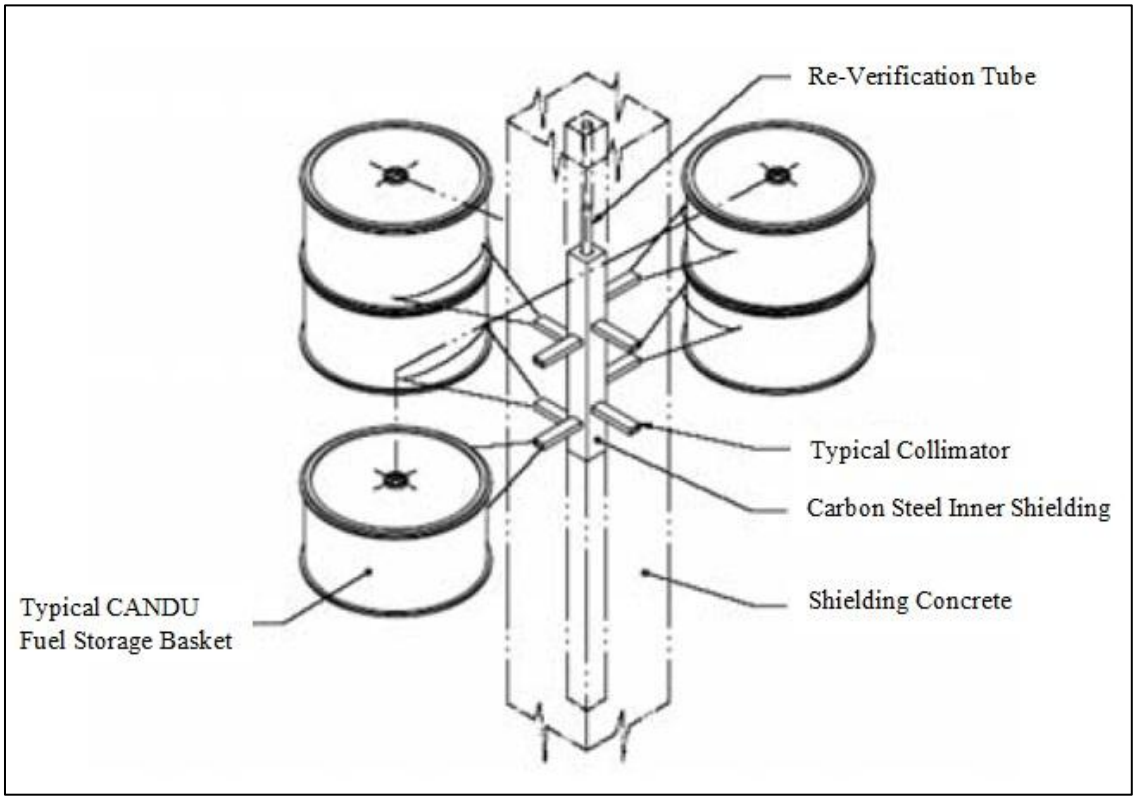

Fig. 4: Arrangement of collimators within MACSTOR KN-400 Re-verification columns

I.E. Previous Work

Gamma and neutron measurements on dry storage casks were conducted by Los Alamos National Laboratory (LANL) for the verification of CANDU spent fuel[10]. The dry storage cask system studied by LANL consisted of stainless steel storage baskets, typically loaded with 60 spent fuel bundles per basket as shown in Fig. 5. The spent fuel storage baskets are stacked into a concrete storage cask, usually 9 storage baskets per

cask. Two re-verification tubes are placed on opposite sides of the cask as shown in Fig. 6. The system is for use in combination with IAEA seals to verify that the contents of a given cask have not changed over time.

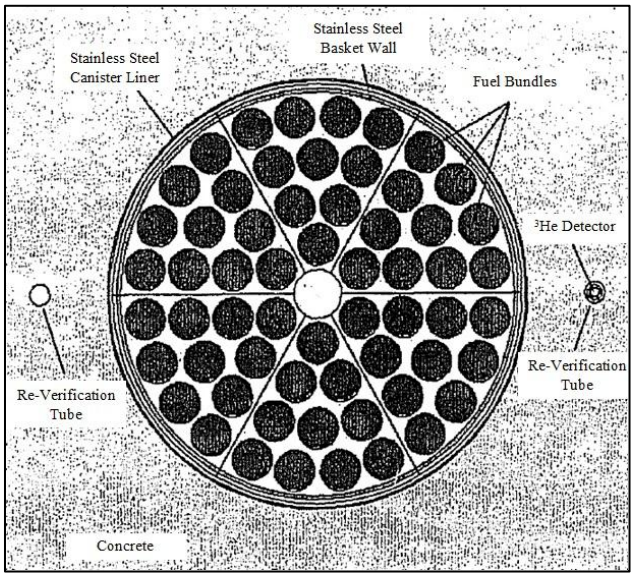

Fig. 5: Top view of the spent-fuel basket inside the storage cask

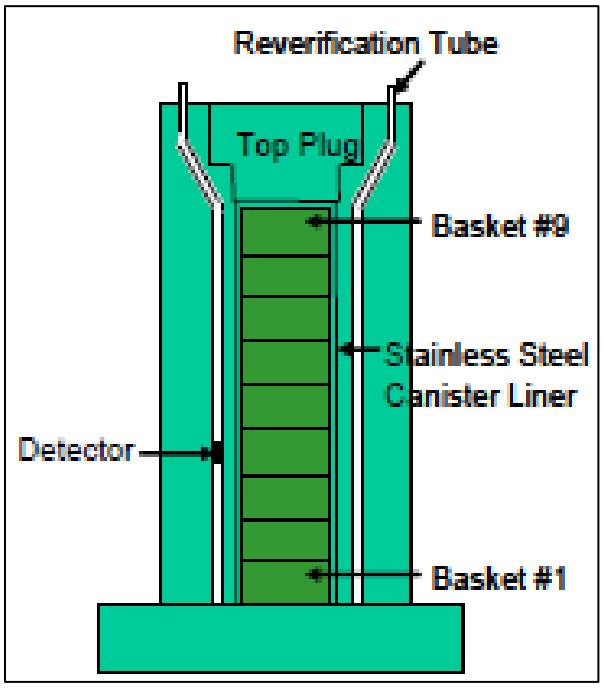

Fig. 6: Side view of CANDU spent-fuel storage cask

LANL performed Monte Carlo transport calculations of neutrons and gamma radiation for one of these CANDU spent fuel casks to compare the performance of proposed neutron and gamma radiation re-verification systems. Three small 4-atm ^{3}He neutron counters were used for neutron measurements and three detectors similar in size and shape to the ^{3}He tube were used for gamma measurements. The conclusions of their work were that the gamma measurements did not provide the necessary sensitivity to safeguard the entire cask and about 70% of the fuel bundles could be removed without any significant reduction in the gamma ray response at the detector. The neutron measurements provided good visibility of the spent fuel to safeguard the entire cask as the measurements can be performed in the two re-verification tubes on the opposite sides of the cask. However, the gamma ray measurement could be effective in monitoring the constant signal level from the spent fuel when continuity of knowledge (COK) is never lost. If there is any failure of the continuous monitoring system, then the re-verification of the spent fuel would require a neutron measurement.

From the discussions above, it can be noticed that the re-verification system planned in MACSTOR KN-400 is substantially different than that of cask and hence the study made by LANL on casks would not hold good for MACSTOR KN-400. Hence, a new evaluation of fingerprinting method for MACSTOR KN-400 is needed.

I.F. Thesis Overview

This thesis studies the evaluation of a gamma and neutron radiation fingerprinting method for spent fuel verification in MACSTOR KN-400 CANDU dry storage facility.

The focus of the study is to determine the sensitivity of the safeguarding system in the MACSTOR KN-400 spent fuel storage facility with respect to different spent fuel bundle diversion cases and to estimate the non-detection probability for the diversion of one significant quantity of plutonium and uranium.

Chapter 2 of this thesis elaborates on the procedures followed for estimating gamma and neutron radiation source term of CANDU6 spent fuel bundle and results of the estimations. Development of MACSTOR KN-400 radiation transport model using general purpose Monte Carlo code, MCNP[4] for both neutron and gamma transport simulations is described in Chapter 3. Chapter 4 describes about gamma radiation transport simulations using the MCNP model. Neutron radiation transport simulations and spent fuel bundle diversion cases studied are described in Chapter 5. Results of the transport simulations and discussions on the results are also made in Chapter 5. This chapter also gives the information about various kinds of spent fuel bundle diversion cases studied to arrive at the radiation detector sensitivities to determine the non-detection probability. Conclusions from the study are made in Chapter 6.

CHAPTER II

RADIATION SOURCE-TERM GENERATION FOR CANDU6 SPENT FUEL BUNDLE

II.A. Gamma and Neutron Radiation Source-term Estimation Using Burnup Code

The expected emission rates of gamma and neutron radiations from the spent fuel stored inside the facility were estimated using ORIGEN-ARP[3] burnup code. However, all the spent fuel bundles stored at the facility will have different material composition, burnups, and cooling times. Therefore, the expected gamma and neutron emission rate was calculated for different burnups of CANDU fuel. The source term estimations were performed using ORIGEN-ARP burnup code contained in the SCALE6 suit of reactor physics codes.

Source term estimations were performed for three different specific powers of 25, 28.39 and 32 MW/tU. The burnup steps of 4, 5, 6, 7, 7.5, 8, 9, and 10 GWD/tU with a cooling period of 10 years was considered. The photon source strength was calculated in 18 energy groups. The radioactivity of individual isotopes available from the ORIGEN output, of which ^{60}Co, ^{137}Cs, ^{154}Eu, and ^{155}Eu were considered explicitly (with their respective photon energies), along with ORIGEN produced 18 group photon energy spectrum for all isotopes. The neutron source strength was estimated for 200 energy groups obtained in ORIGEN-ARP burnup code. The gamma and neutron source strengths estimated using ORIGEN-ARP burnup code for one CANDU spent fuel bundle are shown in Fig. 7 and Fig. 8, respectively. The gamma and neutron energy groups and

respective source strengths are given in Appendix A. These source terms were used in the radiation transport simulations of MACSTOR KN-400 described in the following chapters.

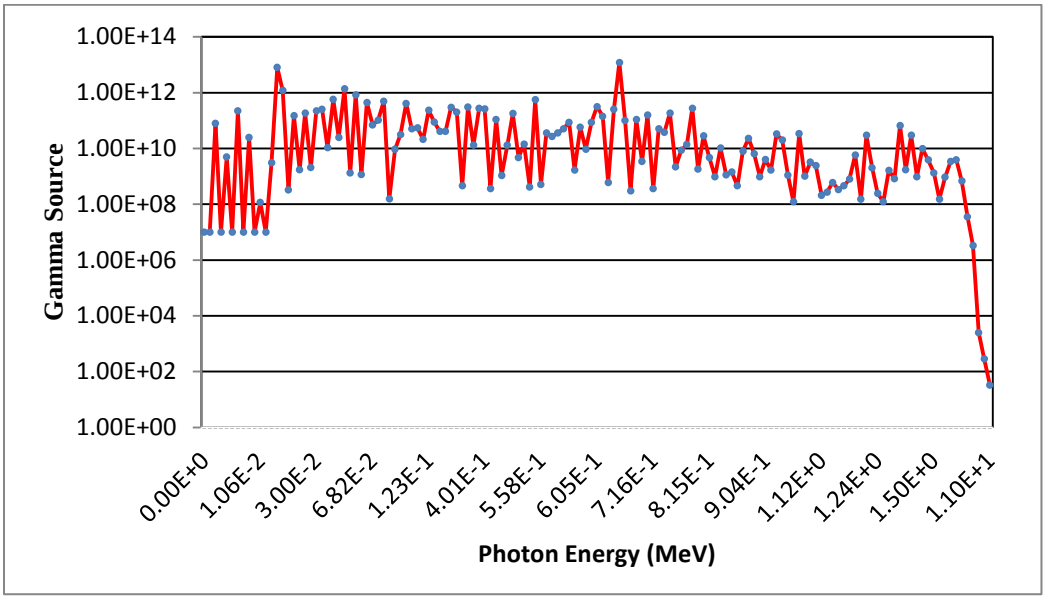

Fig. 7: Photon spectrum for one CANDU-6 spent fuel bundle with discharge Burnup 7.5 GWD/t Burned at Specific Power 28.39 MW/t and cooled for 10 years.

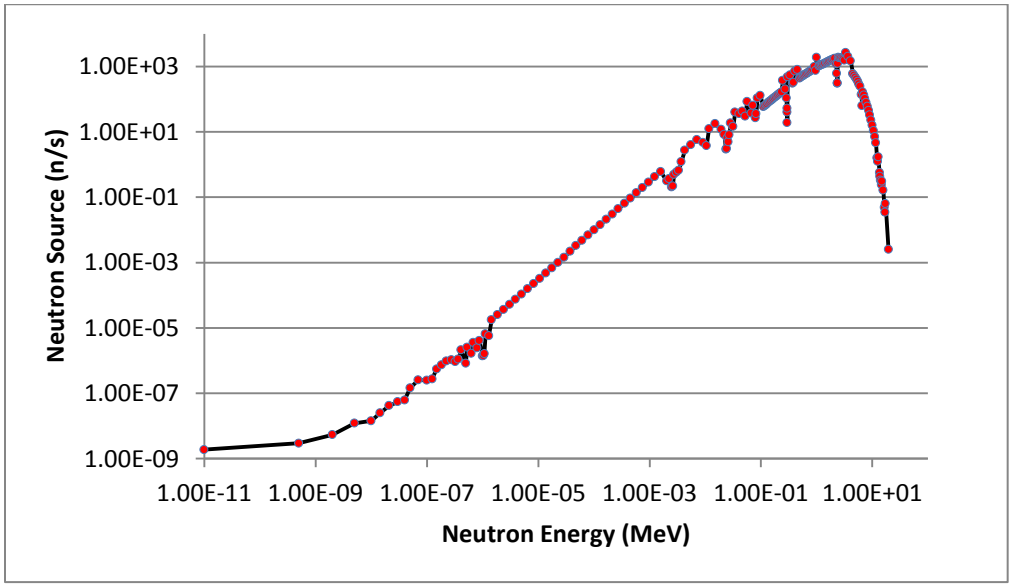

Fig. 8: Neutron spectrum for one CANDU-6 spent fuel bundle with discharge Burnup 7.5 GWD/t Burned at Specific Power 28.39 MW/t and cooled for 10 years.

II.B. Significant Quantity

A Significant Quantity (SQ) is the 'approximate amount of the nuclear material for which possibility of manufacturing a nuclear explosive device cannot be excluded'[11]. It also takes into account of unavoidable losses due to conversion and manufacturing processes. According to International Atomic Energy Agency (IAEA), the significant quantity values currently in use are listed in Table I.

TABLE I

Significant quantities as defined by IAEA[11]

Material	**Significant Quantity**
Direct use nuclear material	
Pu (containing less than 80% ^{238}Pu)	8 kg Pu
^{233}U	8 kg ^{233}U
HEU (^{235}U ≥ 20%)	25 kg ^{235}U
Indirect use nuclear material	
U(^{235}U < 20%) (includes low enriched, natural and depleted uranium)	75 kg ^{235}U (for LEU) (or 10 t natural U or 20 t depleted U)
Th	20 t Th

Direct use nuclear material is that which can be used for manufacture of nuclear explosive devices without transmutation or further enrichment. Whereas, indirect use nuclear material are those materials that require further enrichment or transmutation for use in manufacturing a nuclear explosive device.

From the ORIGEN-ARP burnup calculation, the amounts of the actinides present in a spent fuel bundle after 10 years of cooling are estimated and are provided in Table II.

TABLE II

Amount of actinides present in a 10 years cooled spent fuel bundle

Isotope	**Amount of Actinides in a bundle (kg)**	
	Before irradiation	**10 years cooled spent fuel**
U^{234}	1.06E-03	8.62E-04
U^{235}	1.37E-01	4.25E-02
U^{236}	0.00E+00	1.44E-02
U^{238}	1.91E+01	1.89E+01
Np^{237}	0.00E+00	5.51E-04
Np^{239}	0.00E+00	4.46E-11
Pu^{239}	0.00E+00	4.12E-02
Pu^{240}	0.00E+00	1.32E-02
Pu^{241}	0.00E+00	2.69E-03
Pu^{242}	0.00E+00	1.11E-03

From Table II, it can be observed that the amount of plutonium (Pu) present is about 0.06 kg per bundle. Therefore, to obtain a significant quantity of plutonium (which is 8 kg), it is required to divert at least 138 CANDU6 spent fuel bundles. Also, it is required to divert 1050 CANDU6 spent fuel bundles to get 1 SQ of uranium (20 t depleted uranium).

CHAPTER III

MCNP MODELING OF MACSTOR KN-400 STORAGE FACILITY

III.A. MCNP Model of a CANDU6 Fuel Bundle

The technical specifications of the CANDU fuel bundle used to develop the MCNP models were collected from 'Nuclear Engineering Handbook' by Kenneth D. Kok[5] and 'CANDU6 Technical Summary'[6]. The particle source strength estimated using ORIGEN-ARP and based on the technical data from the literature for a CANDU6 spent fuel bundle with 37 pins, an MCNP model of a CANDU6 spent fuel bundle was developed. A graphic of this model is shown in Fig. 9.

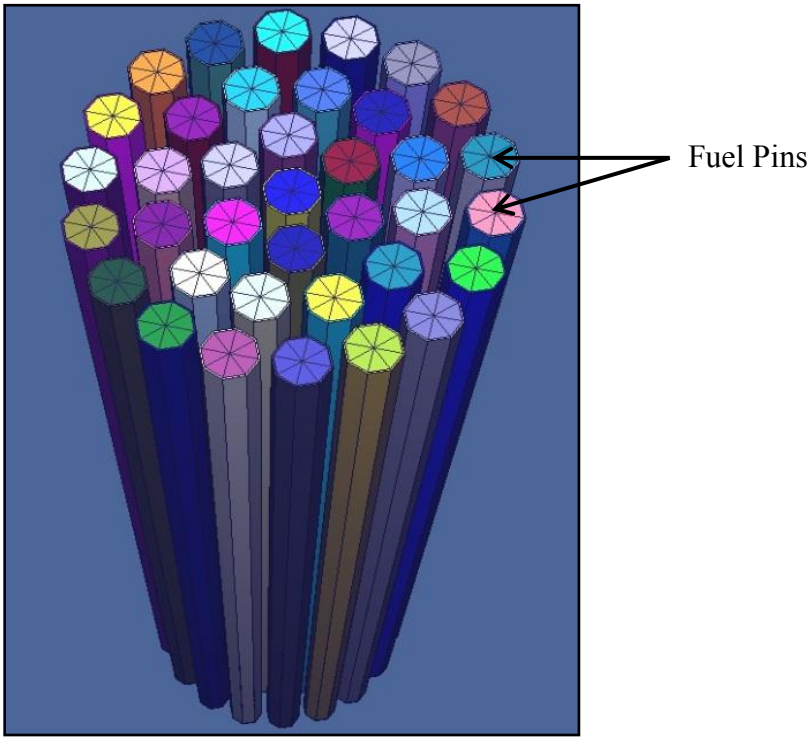

Fig. 9: 3D view of a single 37—pins CANDU 6 fuel bundle model generated by MCNP Visual Editor Software.

III.B. MCNP Model of a Spent Fuel Storage Basket

The MCNP model of a spent fuel storage basket, which can hold 60 CANDU6 fuel bundles, is shown in Fig. 10. This was developed by expanding the MCNP model of a CANDU6 fuel bundle. Carbon steel with density 7.84 g/cc was used as the basket wall material[12]. The position of each fuel bundle inside the storage basket was calculated using the information given in Los Alamos report No. LA-UR-00-2794 on 'Verification of CANDU Spent Fuel in Sealed Storage Casks'[10].

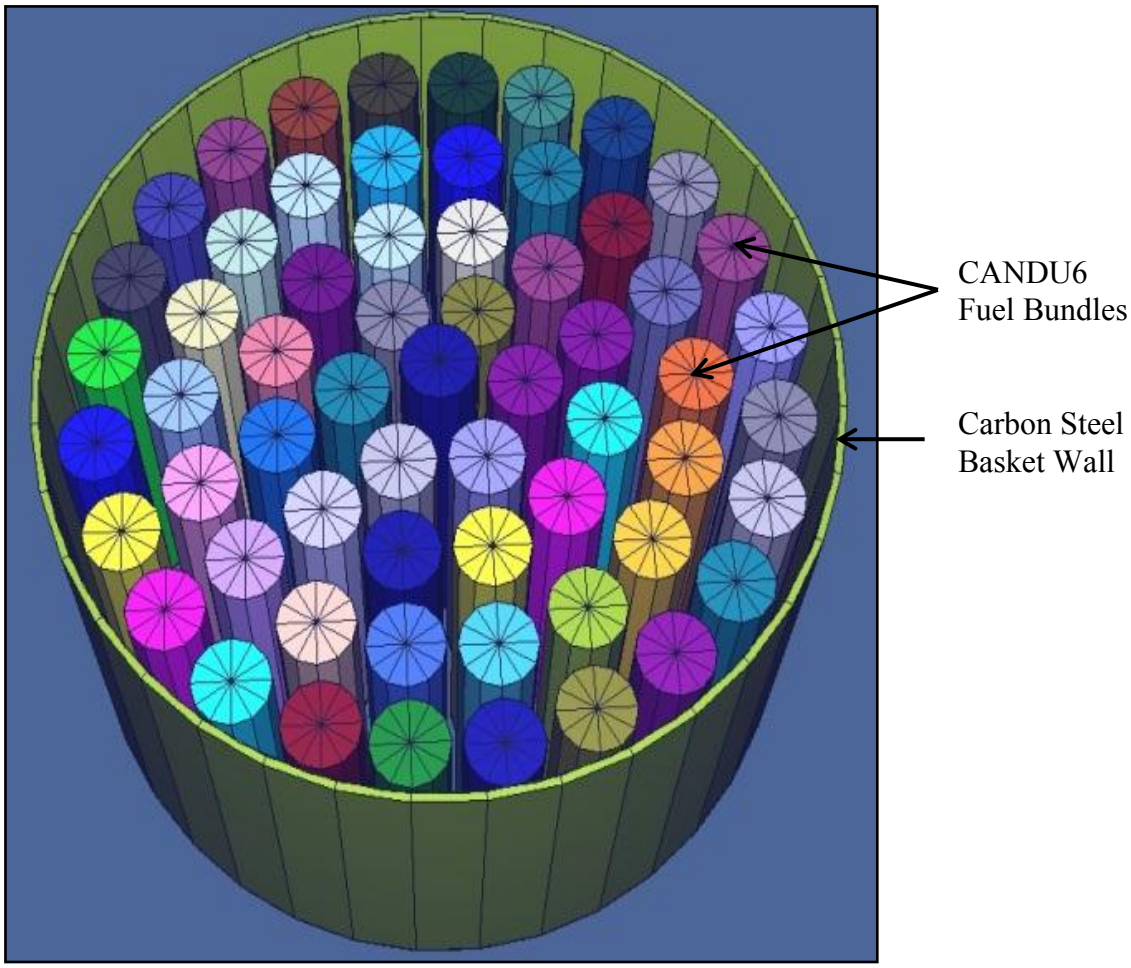

Fig. 10: 3D view of spent fuel storage basket model generated by MCNP Visual Editor Software.

III.C. MCNP Model of a Silo

The MCNP model of spent fuel storage basket was used to develop the model of a silo. The technical data required to develop the model are taken from the document 'Design Description for Re-verification System'[2]. A silo can hold 10 spent fuel storage baskets, containing 600 spent CANDU6 fuel bundles. In a silo, the spent fuel storage baskets are stacked as shown in Fig. 11.

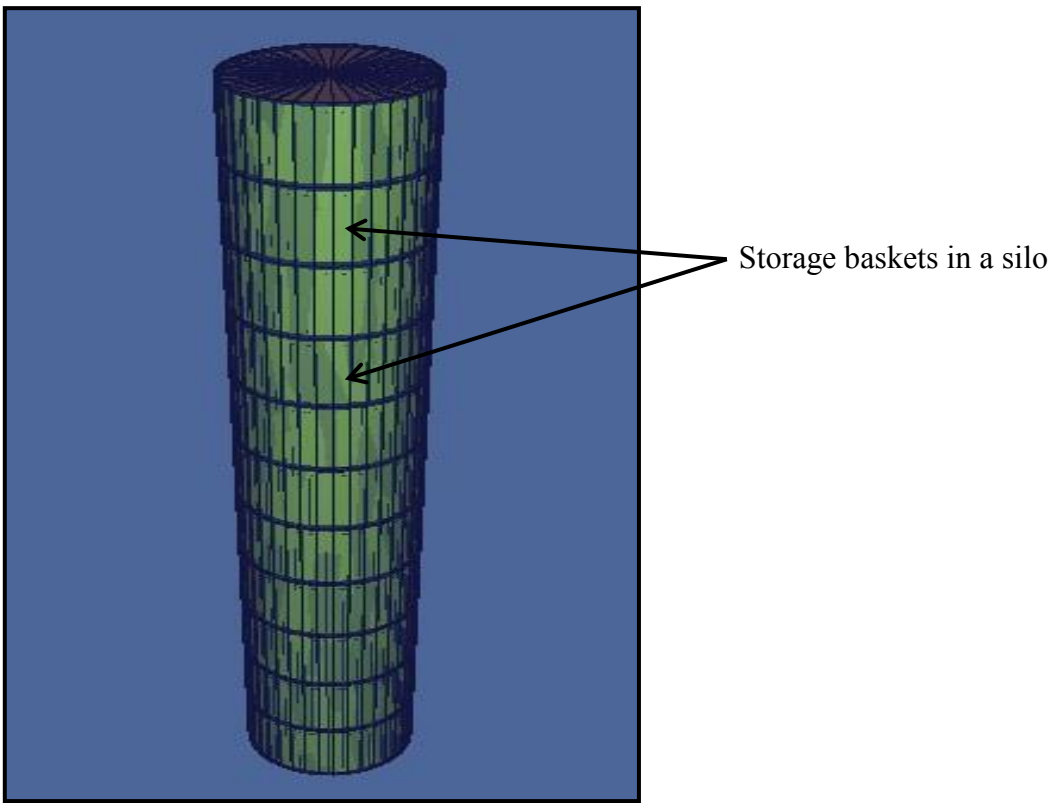

Fig. 11: 3D view of a silo model generated by MCNP Visual Editor Software.

III.D. MCNP Model of the Central Structure of the MACSTOR KN-400 Facility

The central structure of the MACSTOR KN-400 contains four silos with the central re-verification tube along with carbon steel and concrete shield[2]. The re-verification tube

consists of collimators. Collimators are arrayed in a spiral manner along the height of the re-verification tube. Thus 40 collimators (10 in each direction) directing towards the silo looks at all the 40 storage baskets in four silos. MCNP model of a silo was further expanded to develop the central structure of the MACSTOR KN-400 as per the specification. The 3D view of the model generated by MCNP Visual Editor Software, which clearly shows the central re-verification tube, staggered 40 collimators, concrete shield, carbon steel shield, and four silos, is shown in Fig. 12.

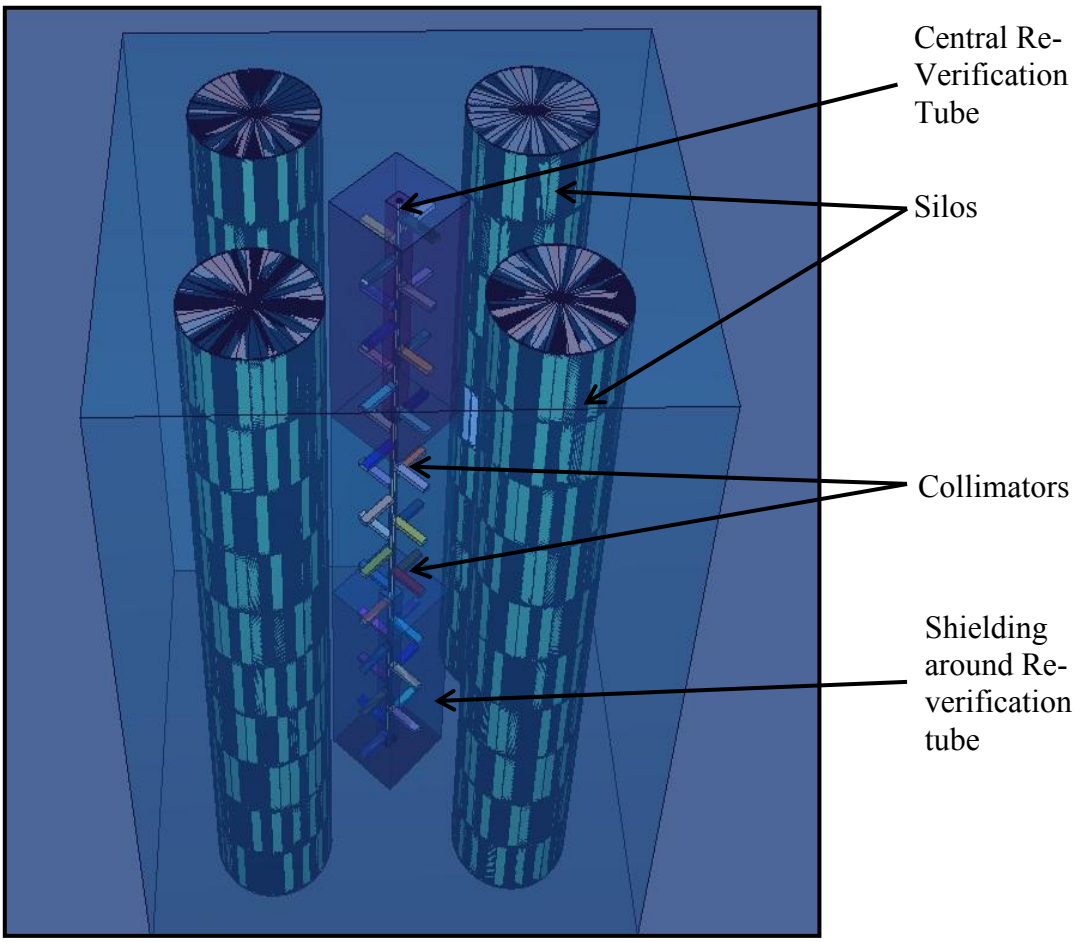

Fig. 12: 3D view of the central structure model generated by MCNP Visual Editor Software.

III.E. MCNP Model of the Peripheral Structure of the MACSTOR KN-400 Facility

The peripheral structure of the MACSTOR KN-400 facility contains four silos, facility concrete walls, and the re-verification tube running inside the module wall for each storage silo[2]. Fig. 13 is a 3D view of the model generated by MCNP Visual Editor Software, which clearly shows the peripheral re-verification tube, module walls, and four silos.

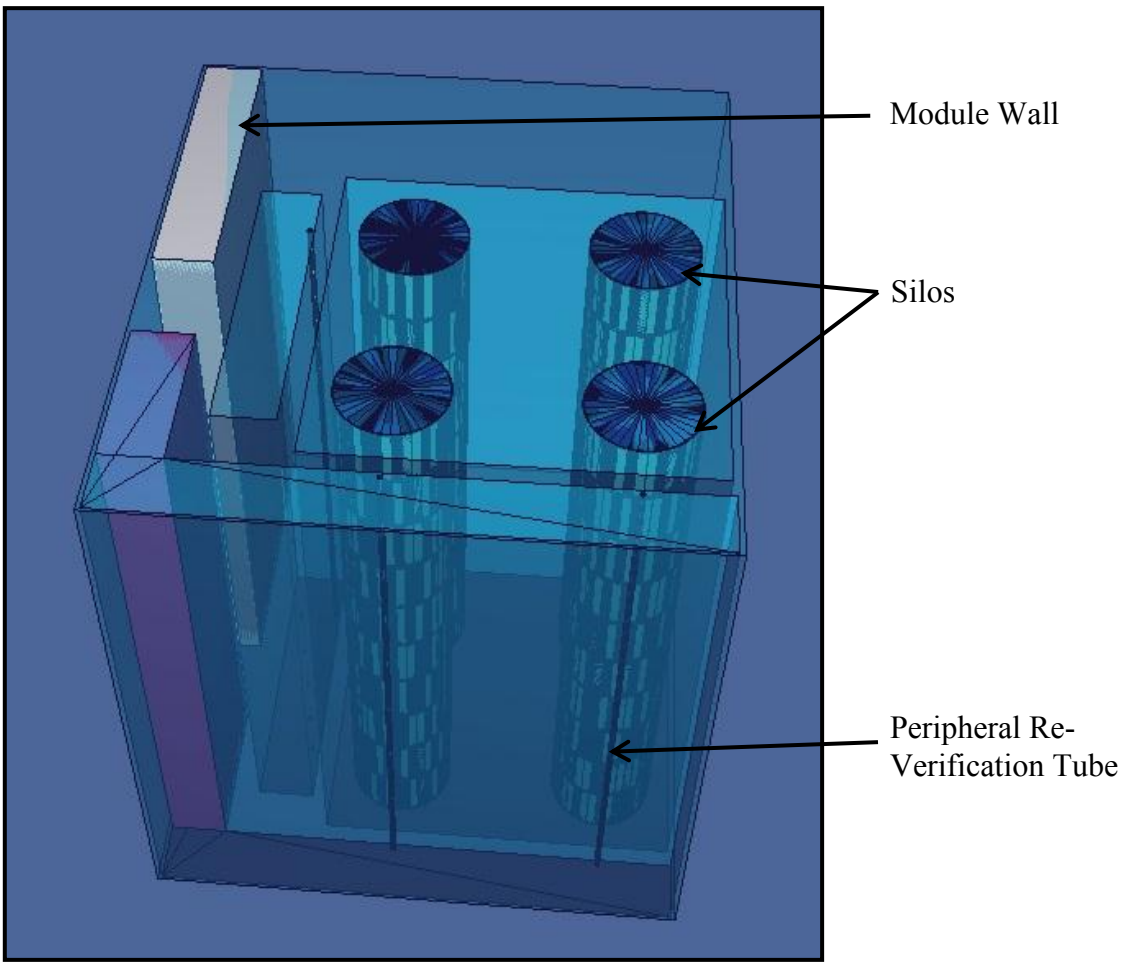

Fig. 13: 3D view of the peripheral structure model generated by MCNP Visual Editor Software.

III.F. MCNP Modeling of Gamma and Neutron Detectors

In the MACSTOR KN-400 facility, the gamma and neutron profile is measured by lowering a detector inside the re-verification tube, which records the radiation signal at the level of each basket. At the top of the re-verification tube, there is a bend to prevent the entrance of any material unknowingly. This bend limits the size of the detector used for the re-verification. The maximum size of the detector that can traverse inside the re-verification tube is 19.05 cm (length) × 3.81 cm (diameter)[10].

The detectors used in real life measurement for gamma radiation measurements is cadmium zinc telluride (CZT) detector[13] and for neutron measurements is helium-3 (^{3}He) neutron counter[14]. In the gamma transport simulations, the size of the CZT detector used was 1.5 cm × 1.5 cm × 0.75 cm. The CZT crystal is placed in an aluminum dioxide cask as shown in Fig. 14.

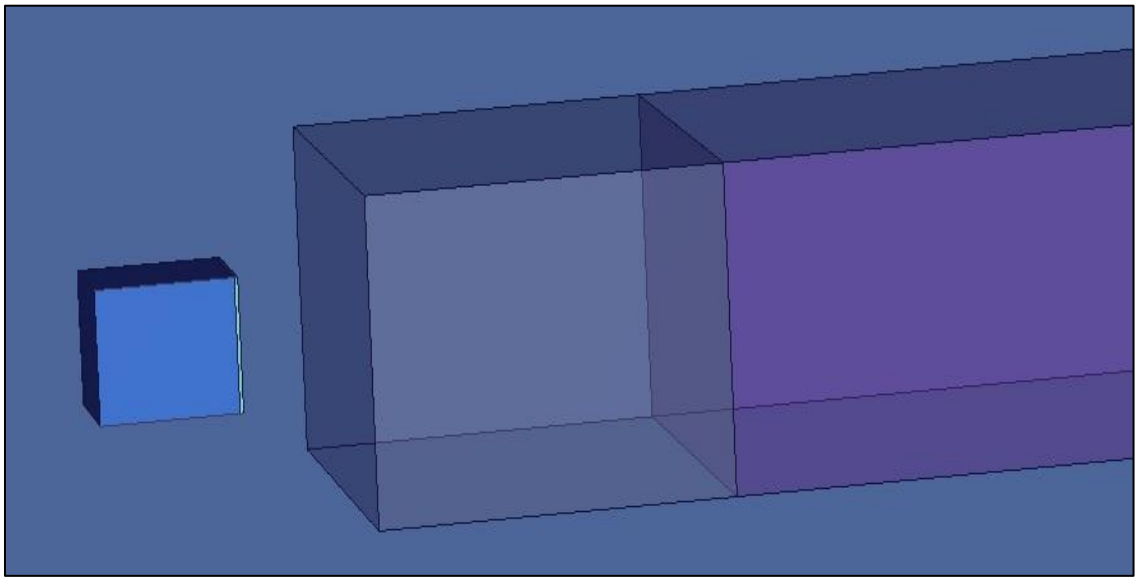

Fig. 14: Image of CZT detector placed in line with the collimator of the re-verification tube

For the neutron transport simulations, ^{3}He neutrons counter with size 6.19 cm (length) × 1.6 cm (diameter), in which the effective length is 2.39 cm and the effective diameter is 1.549 cm was used. Stainless steel was used as a wall material and the ^{3}He gas was kept at 2-atm pressure. The image of the neutron counter used in the simulations is shown in Fig. 15.

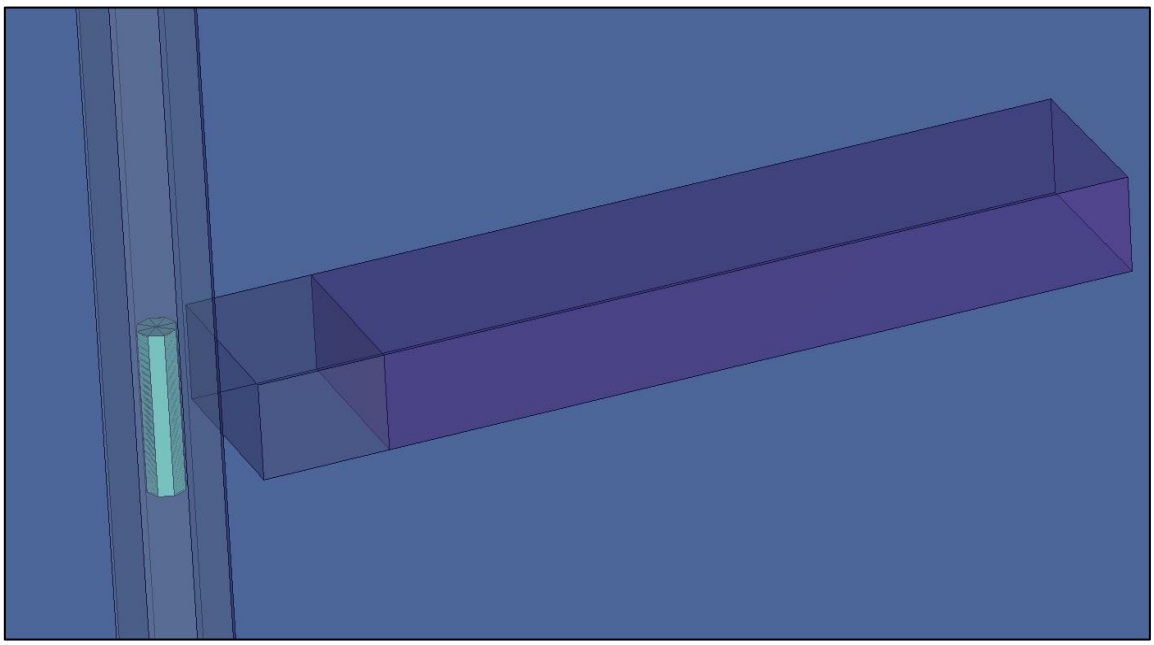

Fig. 15: Image of neutron counter placed in line with the collimator of the re-verification tube

CHAPTER IV

GAMMA RADIATION TRANSPORT SIMULATIONS USING MCNP

The long lived nuclides such as ^{60}Co, ^{137}Cs, ^{154}Eu, and ^{155}Eu were used as reference nuclides for gamma measurements. The 18 energy group gamma source strength estimated using the ORIGEN-ARP burnup code was divided into 140 energy groups, such that energy peak of each interested isotope will be in an energy group. For the simulation, burnup of all the spent fuel bundles contained in the MACSTOR KN-400 storage facility were considered to be same at 7.5 GWD/tU, burned at specific power 28.39 MW/tU and cooled for 10 years.

IV.A. Diversion Analysis Using Central Structure of the MACSTOR KN-400 Facility

For gamma counts measurement inside the re-verification tube, a cadmium zinc telluride (CZT)[13] detector was placed inside the re-verification tube in line with collimator facing a spent fuel storage basket in a silo. The size of the CZT crystal used is 1.5 cm x 1.5 cm x 0.75 cm, as the detector should pass through the bend and move inside the re-verification tube for measurement of gamma counts from all the baskets.

The MCNP simulations were carried out for storage basket with 60 spent fuel bundles in it, which was used as reference case (G-No Diversion case). Two diversion scenarios were considered for the diversion analysis, in the first case (G-Diversion case-1), 9 bundles were removed including 4 bundles from peripheral region of the basket. In

the second case (G-Diversion case-2), the peripheral region bundles were replaced and the bundles from the inner region of the basket were removed. The visual representation of all the cases is shown in Fig. 16.

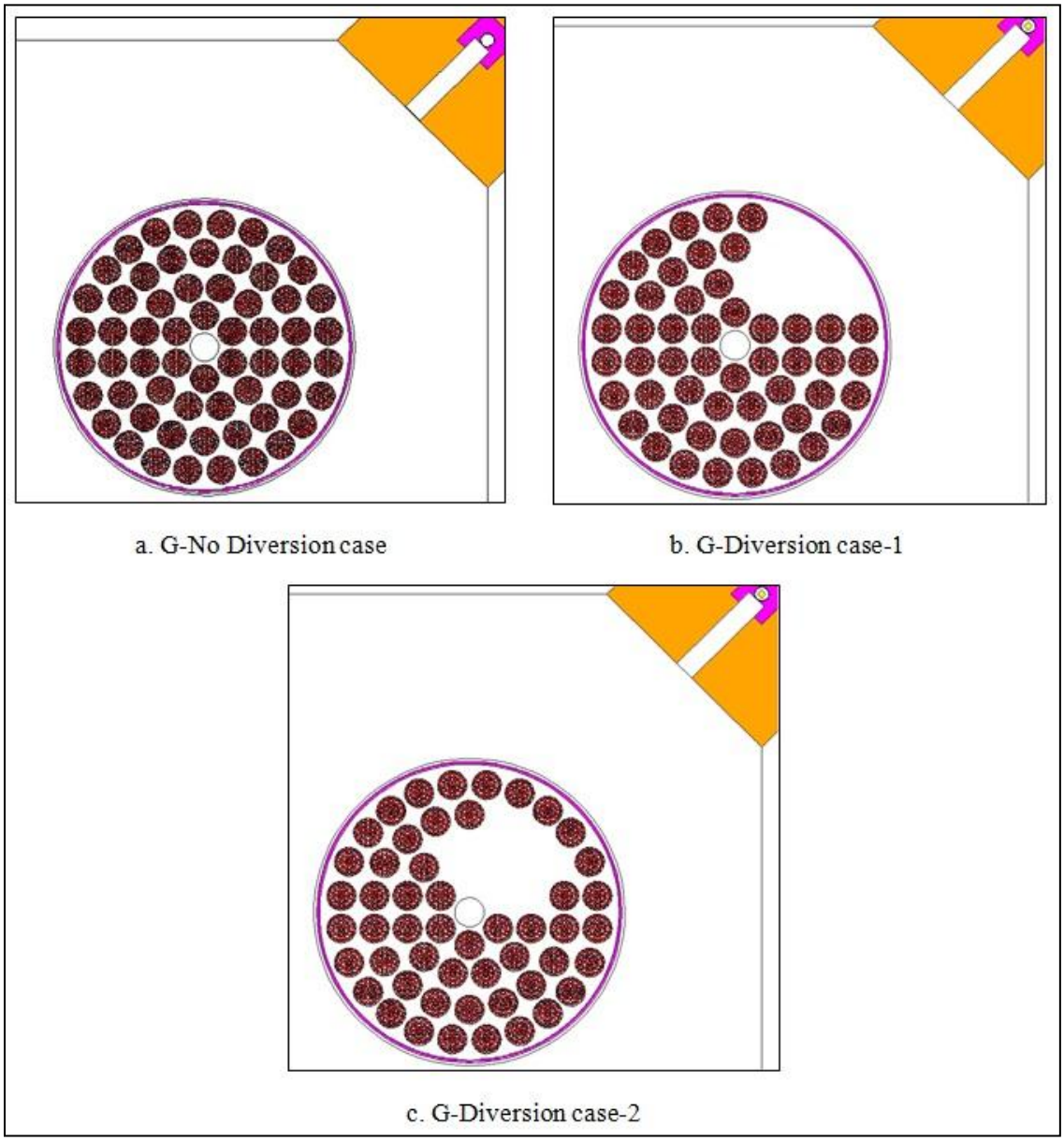

Fig. 16: View of the models used for gamma transport simulation generated by MCNP Visual Editor Software.

The photon spectrum obtained from the MCNP simulation of all the three cases were compared and is shown in Fig. 17. Photon energy peaks from ^{137}Cs (662 keV), ^{154}Eu (723, 876, 996, 1005, and 1274 keV), and ^{60}Co (1173 and 1332 keV) can be noticed from the Fig. 15. From the figure, it can be observed that ^{137}Cs energy peak (662 keV) gives highest response in the detector. Therefore, this region is zoomed in and shown in Fig. 18 for further interpretation of photon signal for the spent fuel bundle diversion cases analysis.

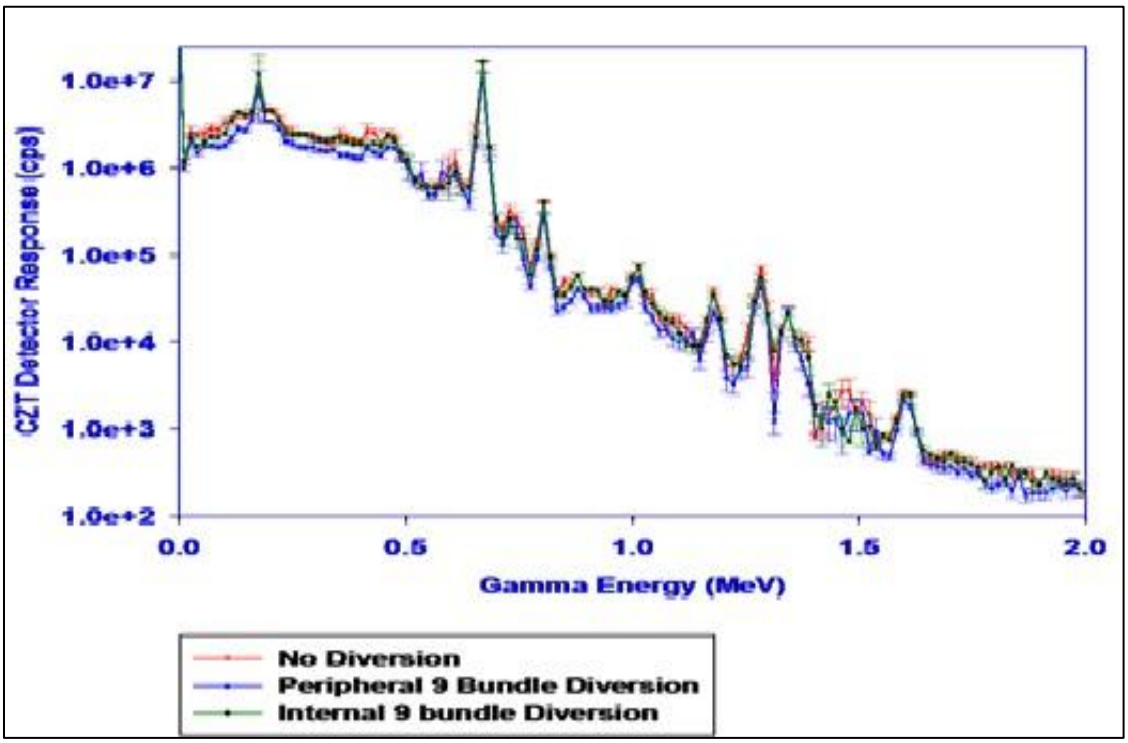

Fig. 17: Photon spectrum in the CZT detector for all the three cases.

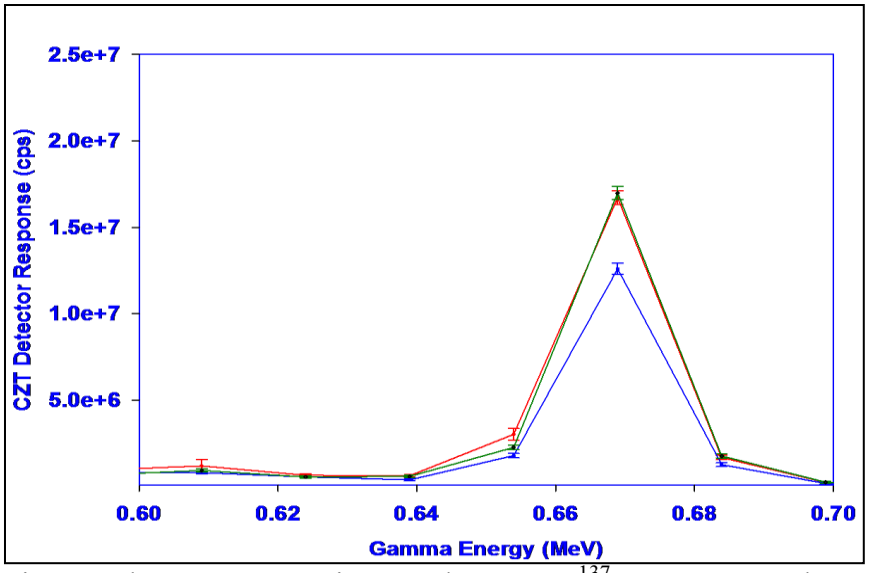

Fig. 18: Photon spectrum in CZT detector at ^{137}Cs energy 662 keV.

From Fig. 18, it can be noticed that the photon signal at energy 662 keV is practically the same for no bundle diversion case (G-No Diversion case) as well as for the case where all the 9 spent fuel bundles were diverted from the inner region (G-Diversion case-2) of the basket. However, spent fuel bundle diversion could be noticed from the 662 keV photon signal degradation (~25%) for the case where 9 bundles were diverted including 4 bundles from the peripheral region (G-Diversion case-1) of the basket.

IV.B. Vertical Gamma Profile of Central Re-verification System

The vertical profile response of the detecting system of MACSTOR KN-400 was studied by modifying the MCNP models. Ten CZT detectors were placed inside the central re-verification tube in line with the collimators facing the spent fuel storage baskets in a silo as shown in Fig. 19. MCNP gamma simulation was performed by

starting the source particles from all the 40 spent fuel storage baskets around the central re-verification tube. For the diversion case, all the 60 spent fuel bundles were removed from one of the baskets and replaced by the dummy bundles made of depleted uranium.

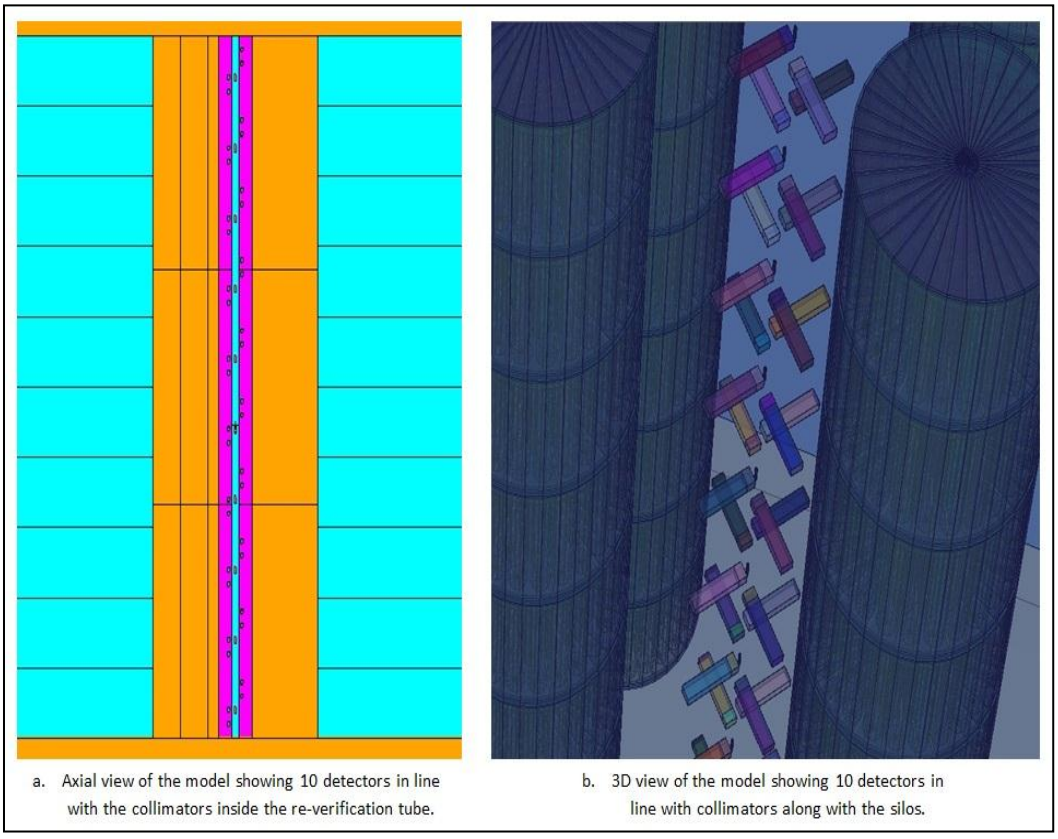

a. Axial view of the model showing 10 detectors in line with the collimators inside the re-verification tube.

b. 3D view of the model showing 10 detectors in line with collimators along with the silos.

Fig. 19: MCNP Visual Editor Software generated view of the model used for vertical gamma profile response of the system.

Total gamma counts obtained at each detector are given in Table III. All 60 spent fuel bundles were removed from a basket in line with the 5th detector for diversion case. From Table III, it can be inferred that detector 5 in line with the diverted basket gave a photon signal reduction by a factor of ~100. Fig. 20 shows the variation in gamma counts at each detector for both the cases.

TABLE III

Gamma counts at each detector inside the central re-verification tube.

Detectors	Gamma counts (γ/s)			
	No Diversion case	% Relative Error	Diversion case	% Relative Error
1 (Bottom)	9.17E+07	4.05	9.43E+07	1.42
2	9.06E+07	2.55	1.00E+08	3.39
3	9.22E+07	4.82	9.55E+07	1.88
4	9.26E+07	8.18	1.08E+08	4.66
5	9.53E+07	7.12	8.24E+05	14.57
6	8.49E+07	1.04	9.74E+07	2.81
7	8.98E+07	3.13	1.02E+08	4.39
8	9.11E+07	4.30	1.00E+08	4.72
9	8.99E+07	3.97	1.10E+08	6.47
10 (Top)	8.85E+07	2.06	9.85E+07	3.47

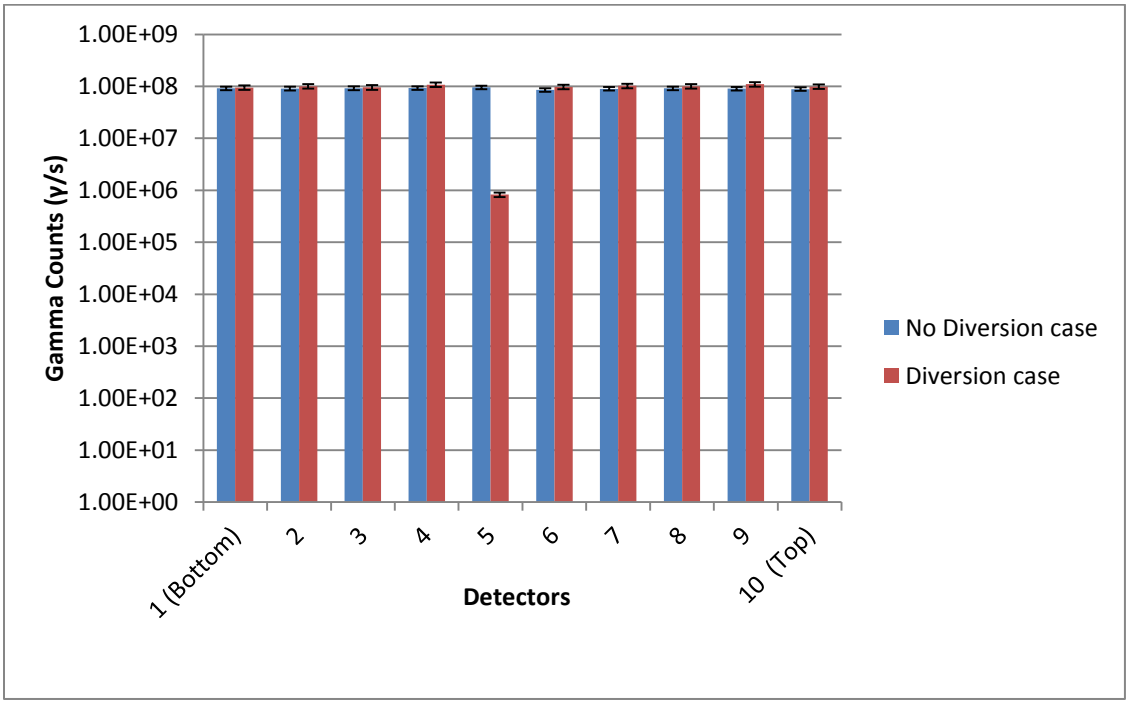

Fig. 20: Gamma counts at each detector inside the re-verification tube.

IV.C. Diversion Analysis Using Peripheral Structure of the MACSTOR KN-400 Facility

For gamma counts measurement inside the peripheral re-verification tube, ten cadmium zinc telluride (CZT)[13] detectors were placed inside the peripheral re-verification tube. MCNP gamma simulations were performed by starting the source particles from the adjacent silos as shown in Fig. 21 and the particles were collected in all 10 detectors inside the peripheral re-verification tube.

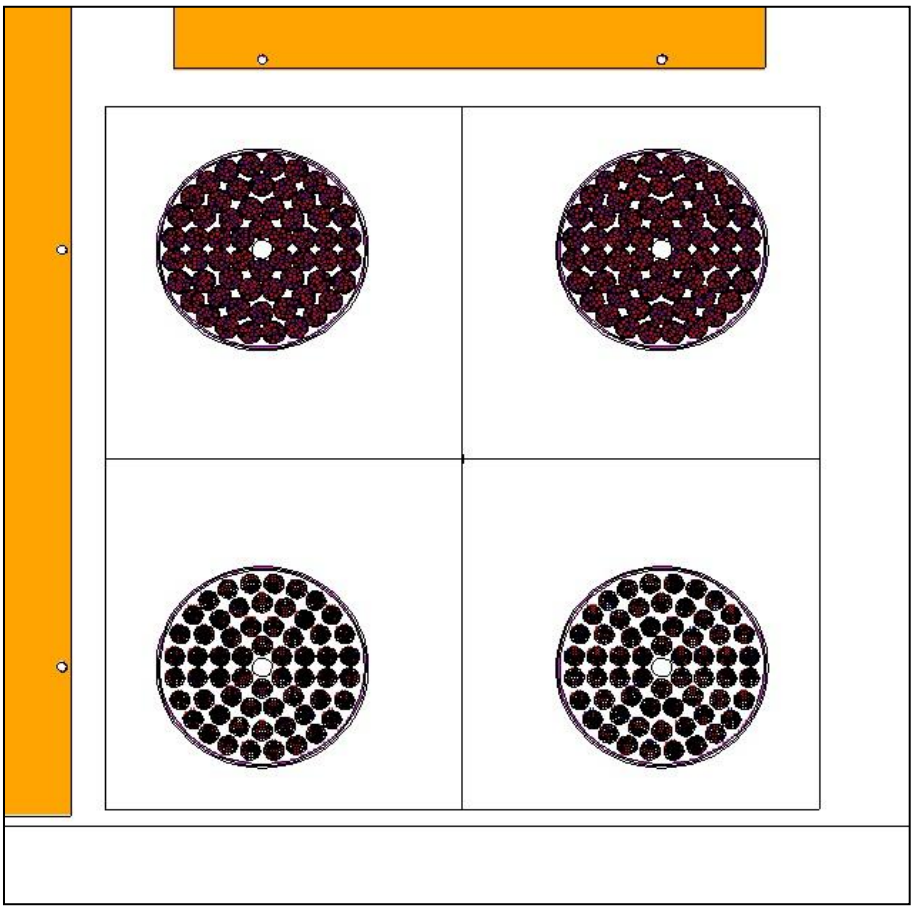

Fig. 21: Plan view of the model showing source particles from the adjacent silos used for vertical gamma profile measurement inside peripheral re-verification tube.

For the diversion case, all 60 spent fuel bundles were removed and replaced by the dummy bundles made of depleted uranium from one of the spent fuel storage baskets in a silo as shown in Fig. 22.

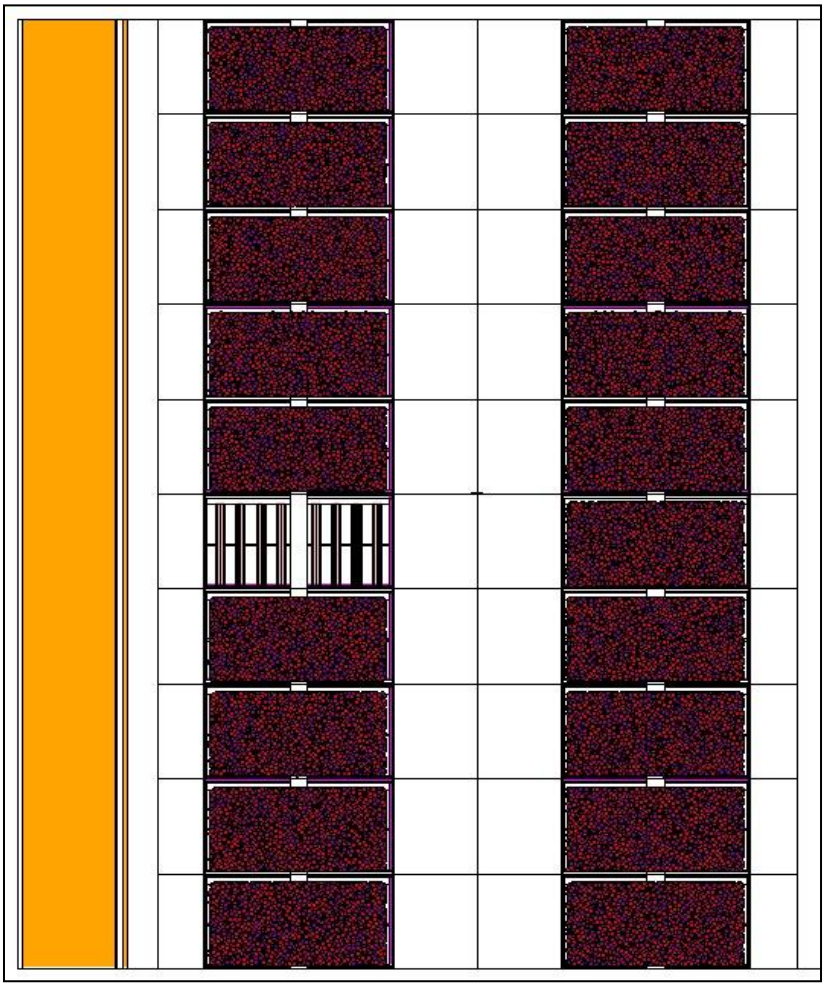

Fig. 22: Axial view of the model showing the diversion of spent fuel bundles from one of the storage baskets.

Total gamma counts obtained at each detector were given in Table IV. All the 60 spent fuel bundles were removed from a basket in line with the 5th detector for diversion

case. From Table IV, it can be inferred that the detector 5 in line with the diverted spent fuel storage basket gave a photon signal reduction by a factor of ~2.5.

TABLE IV

Gamma counts at each detector inside the peripheral re-verification tube

Detectors	**Gamma counts (γ/s)**			
	No Diversion case	**% Relative Error**	**Diversion case**	**% Relative Error**
1 (Bottom)	1.89E+09	5.45	1.86E+09	5.13
2	1.89E+09	5.05	2.70E+09	4.48
3	1.96E+09	4.81	2.23E+09	4.75
4	2.54E+09	4.51	2.12E+09	4.70
5	2.81E+09	6.09	1.26E+09	5.92
6	2.31E+09	4.95	1.54E+09	4.21
7	2.12E+09	5.47	2.08E+09	4.82
8	2.00E+09	4.86	2.52E+09	4.58
9	2.58E+09	4.58	2.70E+09	4.86
10 (Top)	2.12E+09	5.14	2.19E+09	4.72

Fig. 23 shows the variation in gamma counts at each detector inside the peripheral re-verification tube for both the cases. Fig. 20 and Fig. 23 shows that diversion of all the 60 spent fuel bundles from a basket can be detected using gamma measurements. But the results obtained from the gamma simulations showed that it would be difficult to detect the diversion of spent fuel bundles from the inner region of the basket. However, the gamma radiation measurement could be effective for monitoring the constant signal level from the spent fuel when COK is never lost.

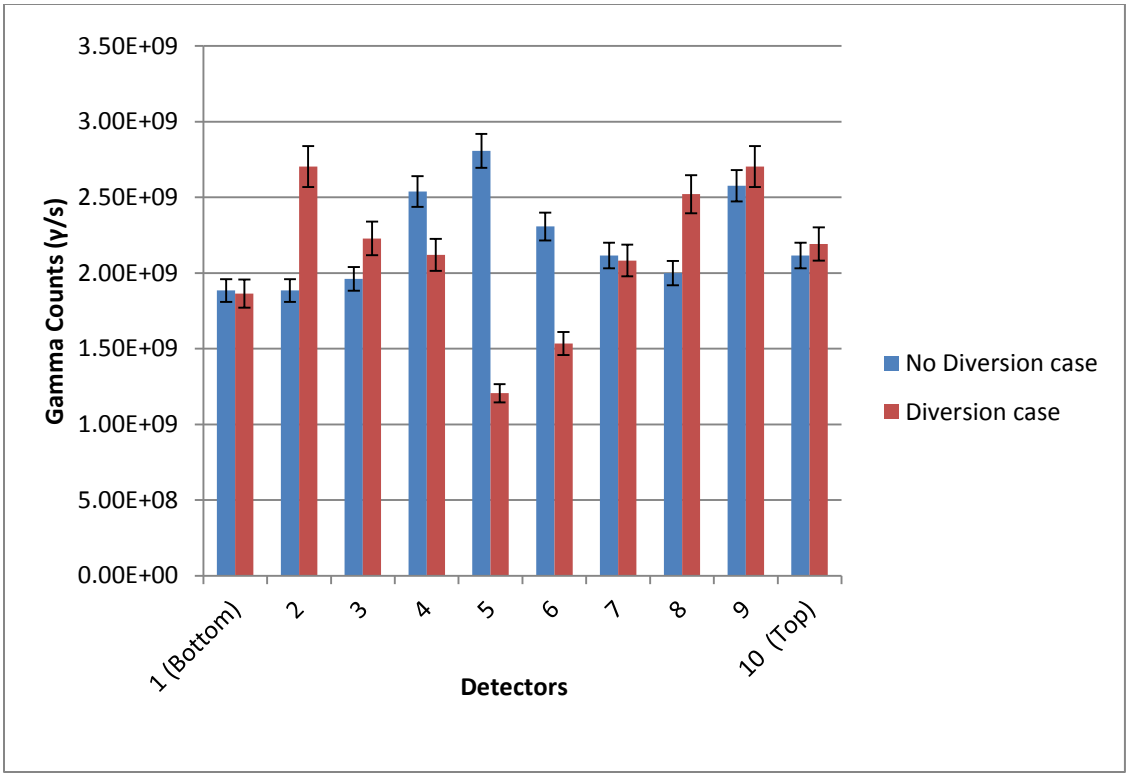

Fig. 23: Gamma counts at each detector inside the peripheral re-verification tube.

CHAPTER V

NEUTRON RADIATION TRANSPORT SIMULATIONS USING MCNP

For the neutron simulations, the fuel bundle with discharge burnup of 7.5 GWD/tU burned at a specific power of 28.39 MW/tU and cooled for 10 years was considered. The neutron source term estimations were completed using ORIGEN-ARP burnup code. The MACSTOR KN-400 MCNP model was developed by incorporating 200 energy group neutron source term obtained using ORIGEN-ARP burnup code. A typical ^{3}He tube neutron detector[14], with thermal neutron sensitivity of 0.6 cps/nv was incorporated into the MCNP model to get the neutron flux in the re-verification tube.

MCNP simulations were performed for no diversion case. The statistical errors associated with the obtained results were very high. Therefore, to reduce the statistical error in the MCNP output, the concrete shielding around the re-verification tube was split into three regions of varying neutron importance as shown in Fig. 24. The energy dependent neutron fluxes obtained at the detector inside the re-verification tube for both the cases are compared in Table V.

The variance reduction method used to reduce the statistical error produced more statistically converged results; therefore, this method was used in the further analysis.

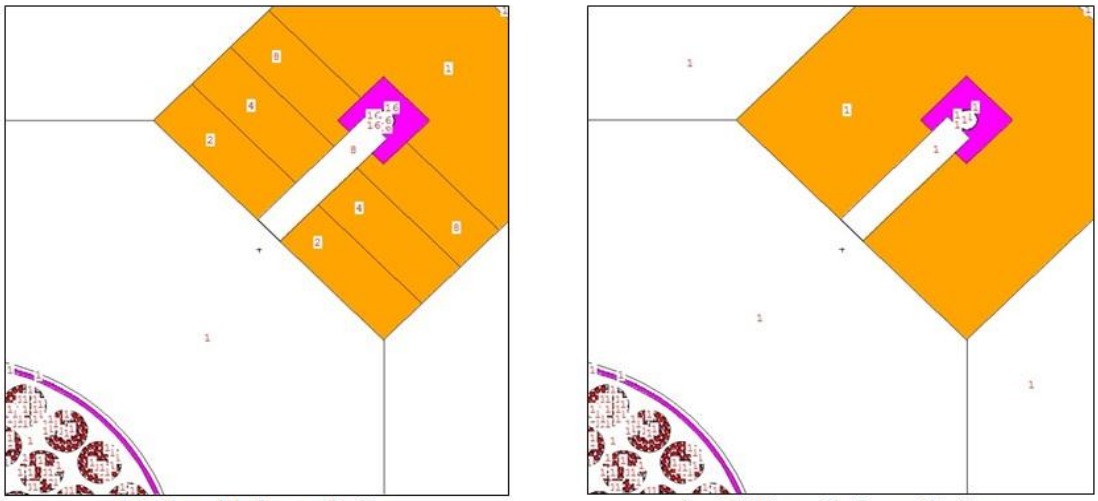

a. MCNP model of re-verification tube concrete structure splitting for neutron importance.

b. MCNP model of re-verification tube concrete structure without splitting for neutron importance.

Fig. 24: View of the models showing concrete structure with and without importance splitting.

TABLE V

Comparison of neutron flux and respective statistical error obtained at the detector for the MCNP models with neutron importance splitting and without importance splitting

Neutron Energy Group (MeV)	**Neutron Flux (n/cm^2-s)**			
	Without neutron importance splitting	**% Statistical Error**	**With neutron importance splitting**	**% Statistical Error**
1.0E-09 to 2.5E-08	5.91E-03	46	7.18E-03	20
2.5E-08 to 5.0E-08	1.70E-02	28	2.66E-02	14
5.0E-08 to 1.4E-07	6.99E-02	24	9.56E-02	10
1.4E-07 to 4.0E-07	1.60E-01	17	1.56E-01	8
4.0E-07 to 1.1E-06	3.11E-01	16	3.11E-01	7
1.1E-06 to 9.1E-03	5.51E+00	6	5.06E+00	3
9.1E-03 to 5.0E-01	5.02E+00	6	4.72E+00	4
5.0E-01 to 2.0E+01	2.42E+00	7	2.66E+00	6
Total	1.35E+01	4	1.30E+01	2

V.A. Diversion Analysis Using Central Structure of the MACSTOR KN-400 Facility

For the diversion analysis, 6 diversion cases were considered along with no diversion case. In the diversion cases, 9 bundles in each case were removed from various regions of the storage basket and replaced by the dummy bundles. The diversion scenarios are:

1. No spent fuel bundle diversion.
2. N-Diversion case-1, where 9 bundles removed including 4 bundles from the peripheral region of the basket facing the collimator.
3. N-Diversion case-2, where 9 bundles removed from the inner region of the basket.
4. N-Diversion case-3, where 3 peripheral bundles were removed from each of the 3 quadrants of the basket (total 9 bundles).
5. N-Diversion case-4, where 3 bundles were removed from inner region of each 3 quadrants of the basket (total 9 bundles).
6. N-Diversion case-5, where 9 bundles were from the right-bottom quadrant of the basket.
7. N-Diversion case-6, where 9 bundles were removed from the left-bottom quadrant, which is opposite to the collimator.

The images of all the diversion scenarios are given in Fig. 25.

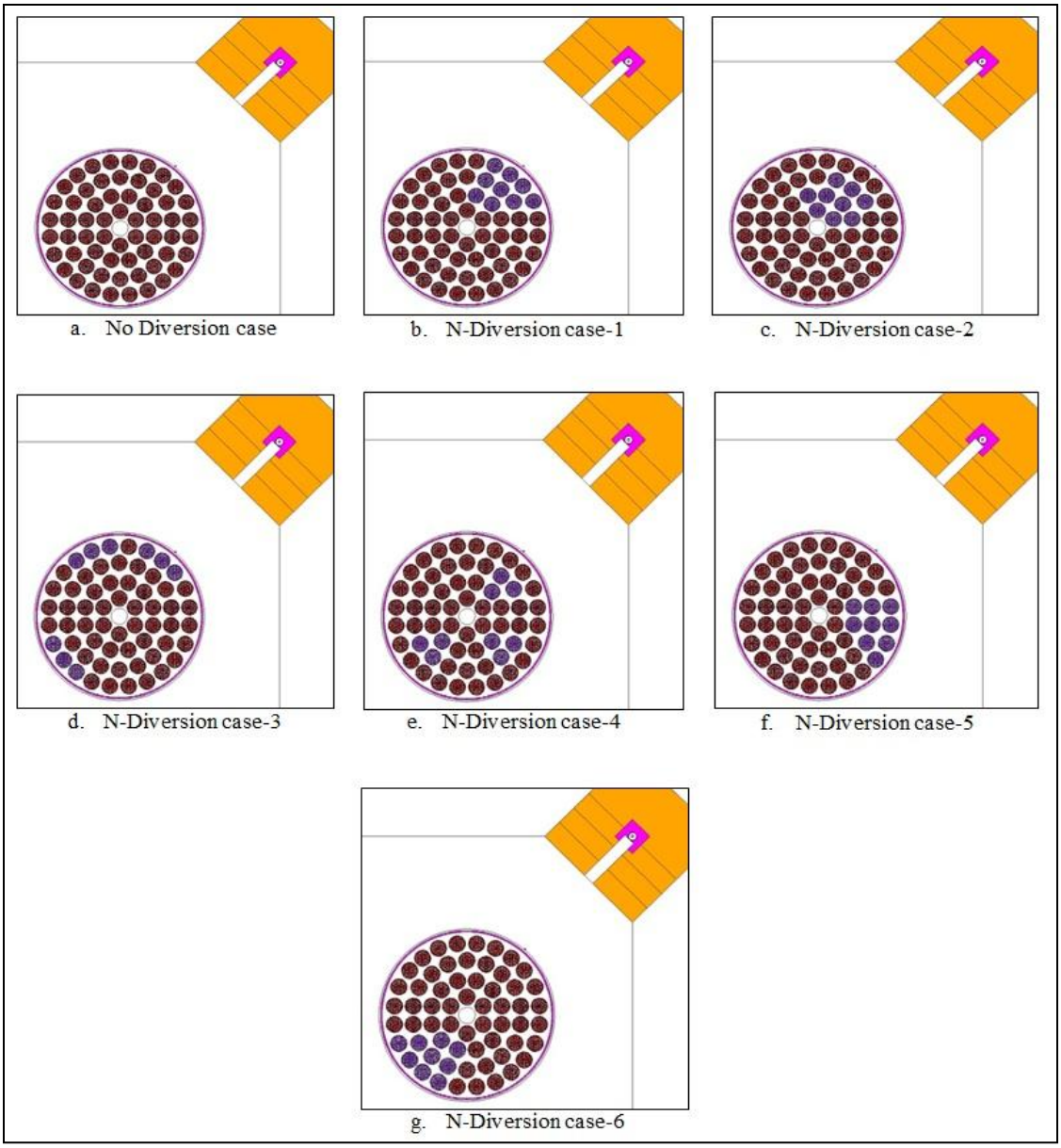

Fig. 25: View of the diversion scenario models used for neutron transport simulation generated by MCNP Visual Editor Software.

The MCNP simulations for all the cases were carried out in two different sets: (1) removed spent fuel bundles were replaced by the dummy bundles made of stainless steel and (2) removed spent fuel bundles were replaced by the dummy bundles made of depleted uranium dioxide.

The energy dependent neutron group fluxes obtained at the detector inside the re-verification tube for the first set, where removed spent fuel bundles were replaced by stainless steel dummy bundles are given in Table VI. The statistical error obtained for all the cases were almost same and are tabulated in the last column of Table VI.

TABLE VI

Neutron flux estimated for diversion scenarios at detector inside re-verification tube for the case where removed spent fuel bundles were replaced by stainless steel dummy bundle.

Neutron Energy Group (MeV)	**Neutron Flux (n/cm^2-s)**			
	No diversion	**Diversion 1**	**Diversion 2**	**Diversion 3**
1.0E-09 to 2.5E-08	1.04E-2	4.22E-3	8.50E-3	5.41E-3
2.5E-08 to 5.0E-08	2.60E-2	1.13E-2	2.34E-2	1.49E-2
5.0E-08 to 1.4E-07	9.04E-2	4.66E-2	6.21E-2	7.38E-2
1.4E-07 to 4.0E-07	1.73E-1	1.27E-1	1.11E-1	1.42E-1
4.0E-07 to 1.1E-06	3.12E-1	1.64E-1	2.02E-1	1.85E-1
1.1E-06 to 9.1E-03	5.22E+0	3.16E+0	3.80E+0	3.88E+0
9.1E-03 to 5.0E-01	4.78E+0	2.73E+0	3.29E+0	3.50E+0
5.0E-01 to 2.0E+01	2.63E+0	1.01E+0	1.78E+0	1.70E+0
Total	1.32E+1	7.26E+0	9.27E+0	9.52E+0
Neutron Energy Group (MeV)	**Neutron Flux (n/cm^2-s)**			
	Diversion 4	**Diversion 5**	**Diversion 6**	**% Statistical Error**
1.0E-09 to 2.5E-08	1.11E-2	6.49E-3	1.14E-2	19.73
2.5E-08 to 5.0E-08	2.02E-2	1.84E-2	2.52E-2	16.85
5.0E-08 to 1.4E-07	7.17E-2	6.76E-2	9.52E-2	10.68
1.4E-07 to 4.0E-07	1.37E-1	1.37E-1	1.67E-1	8.76
4.0E-07 to 1.1E-06	2.20E-1	2.80E-1	2.49E-1	6.10
1.1E-06 to 9.1E-03	4.45E+0	4.10E+0	5.20E+0	2.44
9.1E-03 to 5.0E-01	3.74E+0	3.91E+0	4.50E+0	2.88
5.0E-01 to 2.0E+01	2.16E+0	2.09E+0	2.55E+0	4.25
Total	1.08E+1	1.06E+1	1.28E+1	1.70

The neutron energy dependent group fluxes for all the 6 diversion cases and no diversion case for first set, where removed spent fuel bundles were replaced by the stainless steel dummy bundles are depicted in Fig. 26.

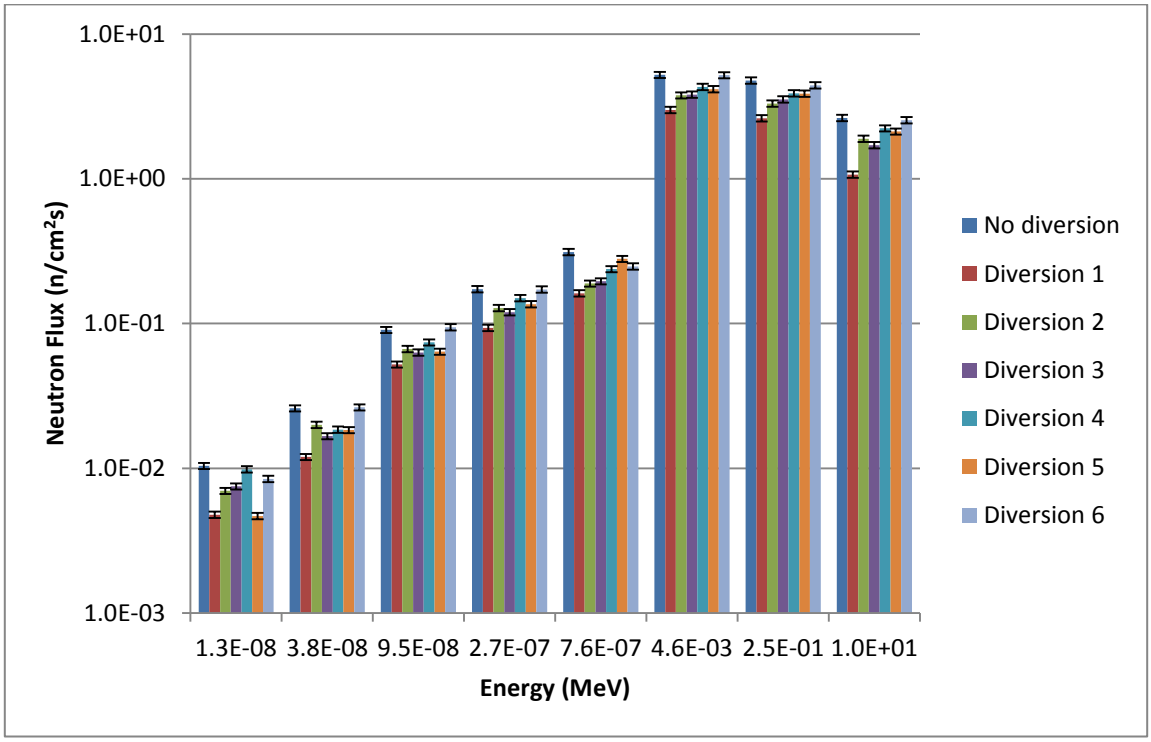

Fig. 26: Comparison of neutron fluxes for 6 diversion scenarios and no diversion scenario for the first set.

The energy dependent neutron group fluxes obtained at the detector inside the re-verification tube for the second set, where removed spent fuel bundles were replaced by depleted uranium dioxide dummy bundles are given in Table VII. The statistical errors obtained are tabulated in the last column of Table.

TABLE VII

Neutron flux estimated for diversion scenarios at detector inside re-verification tube for the case where removed spent fuel bundles were replaced by depleted uranium dioxide dummy bundle.

Neutron Energy Group (MeV)	**Neutron Flux (n/cm^2-s)**			
	No diversion	**Diversion 1**	**Diversion 2**	**Diversion 3**
1.0E-09 to 2.5E-08	1.04E-2	4.78E-3	6.99E-3	7.51E-3
2.5E-08 to 5.0E-08	2.60E-2	1.20E-2	2.00E-2	1.67E-2
5.0E-08 to 1.4E-07	9.04E-2	5.22E-2	6.68E-2	6.32E-2
1.4E-07 to 4.0E-07	1.73E-1	9.35E-2	1.28E-1	1.20E-1
4.0E-07 to 1.1E-06	3.12E-1	1.62E-1	1.89E-1	1.96E-1
1.1E-06 to 9.1E-03	5.22E+0	2.99E+0	3.77E+0	3.82E+0
9.1E-03 to 5.0E-01	4.78E+0	2.62E+0	3.31E+0	3.54E+0
5.0E-01 to 2.0E+01	2.63E+0	1.07E+0	1.89E+0	1.71E+0
Total	1.32E+1	7.00E+0	9.35E+0	9.44E+0
Neutron Energy Group (MeV)	**Neutron Flux (n/cm^2-s)**			
	Diversion 4	**Diversion 5**	**Diversion 6**	**% Statistical Error**
1.0E-09 to 2.5E-08	9.86E-3	4.69E-3	8.47E-3	17.28
2.5E-08 to 5.0E-08	1.85E-2	1.84E-2	2.64E-2	19.78
5.0E-08 to 1.4E-07	7.41E-2	6.40E-2	9.44E-2	12.31
1.4E-07 to 4.0E-07	1.50E-1	1.36E-1	1.72E-1	10.57
4.0E-07 to 1.1E-06	2.38E-1	2.80E-1	2.48E-1	6.84
1.1E-06 to 9.1E-03	4.31E+0	4.16E+0	5.19E+0	2.77
9.1E-03 to 5.0E-01	3.89E+0	3.88E+0	4.43E+0	3.23
5.0E-01 to 2.0E+01	2.23E+0	2.12E+0	2.54E+0	4.81
Total	1.10E+1	1.06E+1	1.28E+1	1.92

The neutron energy dependent group fluxes for all the 6 diversion scenario cases and no diversion case for first set, where removed spent fuel bundles were replaced by the depleted uranium dioxide dummy bundles are depicted in Fig. 27.

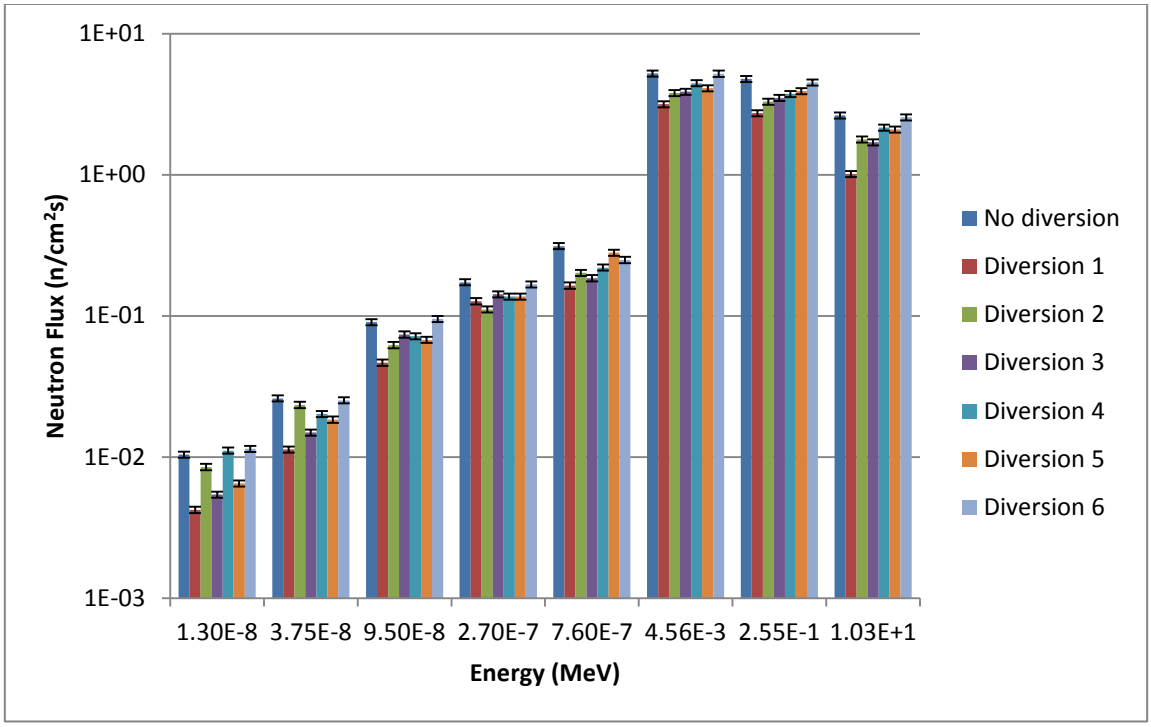

Fig. 27: Comparison of neutron fluxes for 6 diversion scenarios and no diversion scenario for the second set.

From Tables VI and VII, it can be observed that most neutron signal reduction is observed for diversion case-1 (by a factor of 2). If the neutron signal reductions are ordered from most to least, the pattern will be diversion case 1, 2, 3, 5, 4, 6. Diversion case 6 has the very low signal difference (practically no difference) compared to the no diversion case.

From Tables VI and VII and the pictorial representations, it can be observed that the neutron flux obtained was dominated by fast neutrons, but the ^{3}He detector used inside the re-verification tube is highly responsive to thermal neutrons than fast neutrons. The energy of the fast neutrons can be reduced by slowing it down by using the thermalizing material between the detector and spent fuel basket. Therefore, MCNP models were

modified to thermalize the fast neutrons by adding 2 inch thick thermalizing material inside the collimator. SWX-213 (Pure Polyethylene)[15] was used as the thermalizing material with the material density 0.92 g/cc. MCNP simulations were carried out in two steps: (1) 2-inch polyethylene inside the collimator at the detector end, and (2) 2-inch polyethylene inside the collimator at the basket end. Images of the two models are shown in Fig. 28.

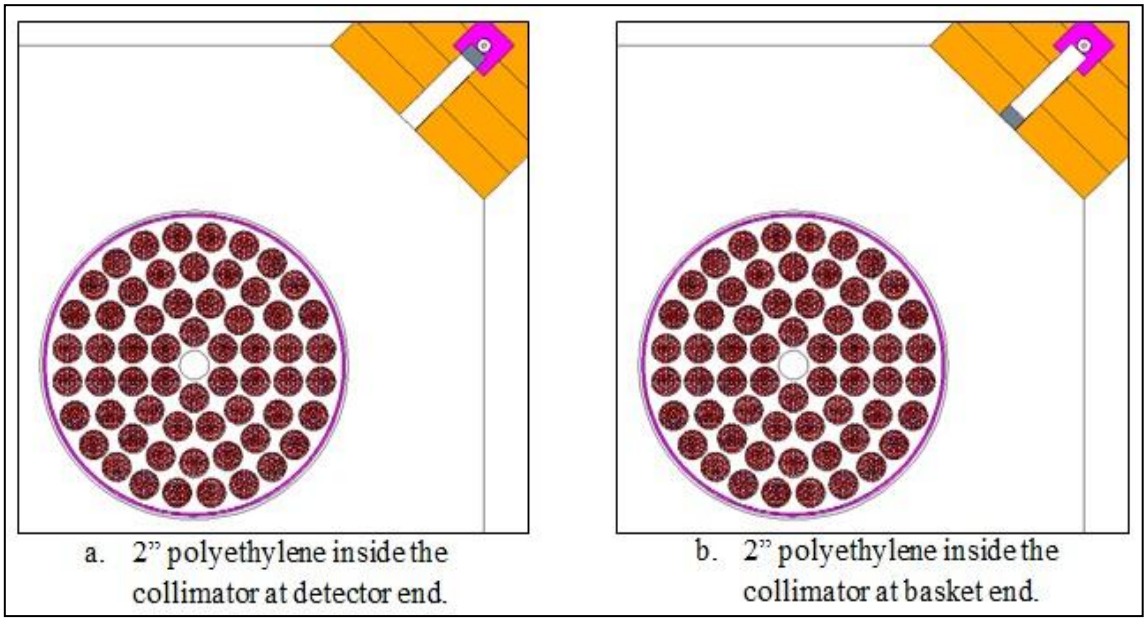

Fig. 28: Images showing the position of polyethylene inside the collimator

The comparison of energy dependent neutron group fluxes obtained at the detector inside the re-verification tube for the cases where, no polyethylene inside the collimator, 2" polyethylene inside the collimator at detector end, and 2" polyethylene inside the collimator at basket end are given in Table VIII.

TABLE VIII
Neutron flux estimated at the detector inside re-verification tube for no diversion case.

Neutron Energy Group (MeV)	Neutron Flux (n/cm^2-s)					
	No polyethy-lene	% Statist-ical Error	Polyeth-ylene at detector end	% Statistic-al Error	Polyethy-lene at basket end	% Statistic-al Error
1.0E-9 to 2.5E-8	6.59E-02	22.03	4.32E-01	2.96	6.67E-02	9.71
2.5E-8 to 5.0E-8	1.91E-01	12.53	8.88E-01	2.12	1.63E-01	5.80
5.0E-8 to 1.4E-7	5.69E-01	7.05	1.82E+0	1.55	5.89E-01	3.18
1.4E-7 to 4.0E-7	1.18E+00	5.14	1.46E+0	1.70	1.16E+00	2.45
4.0E-7 to 1.1E-6	2.21E+00	4.19	2.05E+0	1.50	2.09E+00	1.86
1.1E-6 to 9.1E-3	3.87E+01	1.61	3.04E+0	0.56	3.66E+01	0.68
9.1E-3 to 5.0E-1	2.81E+01	2.18	2.17E+0	0.74	2.59E+01	0.87
5.0E-1 to 2.0E+1	9.62E+00	4.11	6.94E+0	1.34	8.13E+00	1.67
Total	8.06E+01	1.24	6.57E+0	0.42	7.47E+01	0.50

Fig. 29 schematically shows the variation of neutron flux with respect to neutron energy for all the above mentioned cases.

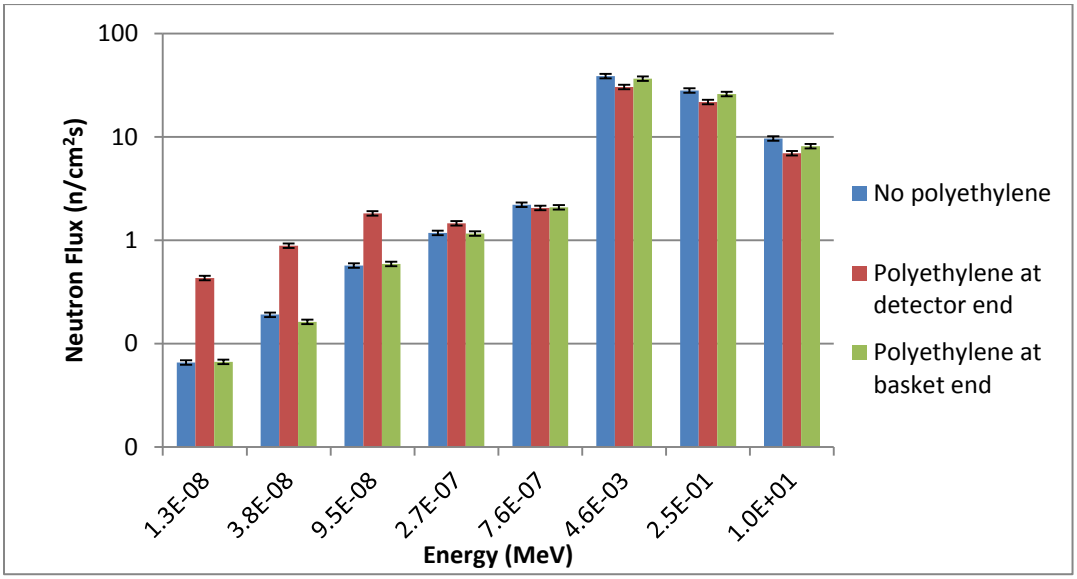

Fig. 29: Schematic representation of neutron flux variation for the cases with and without polyethylene inside the collimator.

From Table VIII and Fig. 29, it can be observed that better neutron fluxes in thermal region were obtained for the MCNP simulation in the case where 2" polyethylene inside the collimator at detector end than no polyethylene case and 2" polyethylene inside the collimator at basket end case. Therefore, all the further MCNP neutron simulations were performed using the model with 2" polyethylene inside the collimator at detector end.

N-Diversion case-6 (refer Fig. 25), where 9 spent fuel bundles were removed from the left-bottom quadrant, which gave very low signal difference (practically no difference) compared to the no diversion case was considered to check the effect of polyethylene inclusion. The MCNP simulations were carried out for two cases; (1) removed spent fuel bundles were replaced by stainless steel dummy bundles, and (2) removed spent fuel bundles were replaced by depleted uranium dioxide dummy bundles as shown in Fig. 30.

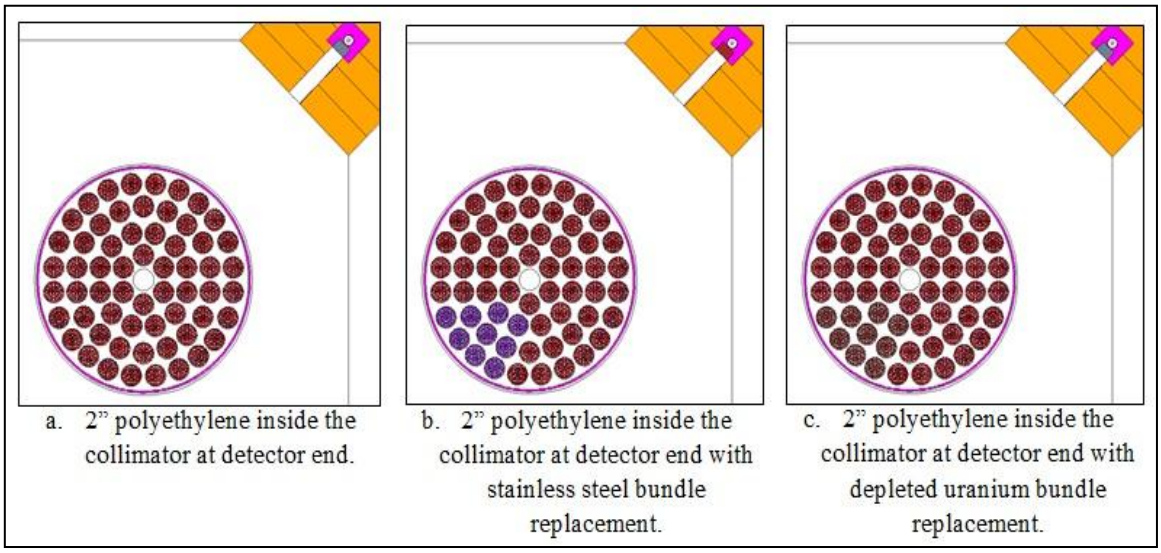

Fig. 30: MCNP models used to check the effect of inclusion of polyethylene inside the collimator.

The comparison of the energy dependent neutron group fluxes obtained at the detector inside the re-verification tube for no diversion case and diversion cases (N-Diversion case-6) with dummy bundles replacement are given in Table IX.

TABLE IX

Neutron flux estimated at the detector inside re-verification tube for no diversion case and diversion cases.

Neutron Energy Group (MeV)	**Neutron Flux (n/cm^2-s)**					
	No Diversion	**% Statistic-al Error**	**Stainless steel bundle replace-ment**	**% Statistic-al Error**	**Depleted uranium bundle replace-ment**	**% Statistic-al Error**
1.0E-9 to 2.5E-8	4.32E-01	2.96	4.33E-01	3.59	4.34E-01	3.59
2.5E-8 to 5.0E-8	8.88E-01	2.12	8.78E-01	2.65	8.78E-01	2.65
5.0E-8 to 1.4E-7	1.82E+00	1.55	1.79E+0	1.93	1.78E+0	1.93
1.4E-7 to 4.0E-7	1.46E+00	1.70	1.45E+0	2.23	1.45E+0	2.23
4.0E-7 to 1.1E-6	2.05E+00	1.50	2.04E+0	1.98	2.04E+0	1.97
1.1E-6 to 9.1E-3	3.04E+01	0.56	3.01E+0	0.72	3.01E+0	0.72
9.1E-3 to 5.0E-1	2.17E+01	0.74	2.16E+0	0.91	2.16E+0	0.91
5.0E-1 to	6.94E+00	1.34	6.81E+0	1.66	6.82E+0	1.66
Total	6.57E+01	0.42	6.51E+0	0.52	6.51E+0	0.52

Fig. 31 shown below schematically represents the neutron flux variation with respect to neutron energy for no diversion case, diversion case with stainless steel dummy bundles replacement, and diversion case with dummy depleted uranium dioxide bundles replacement.

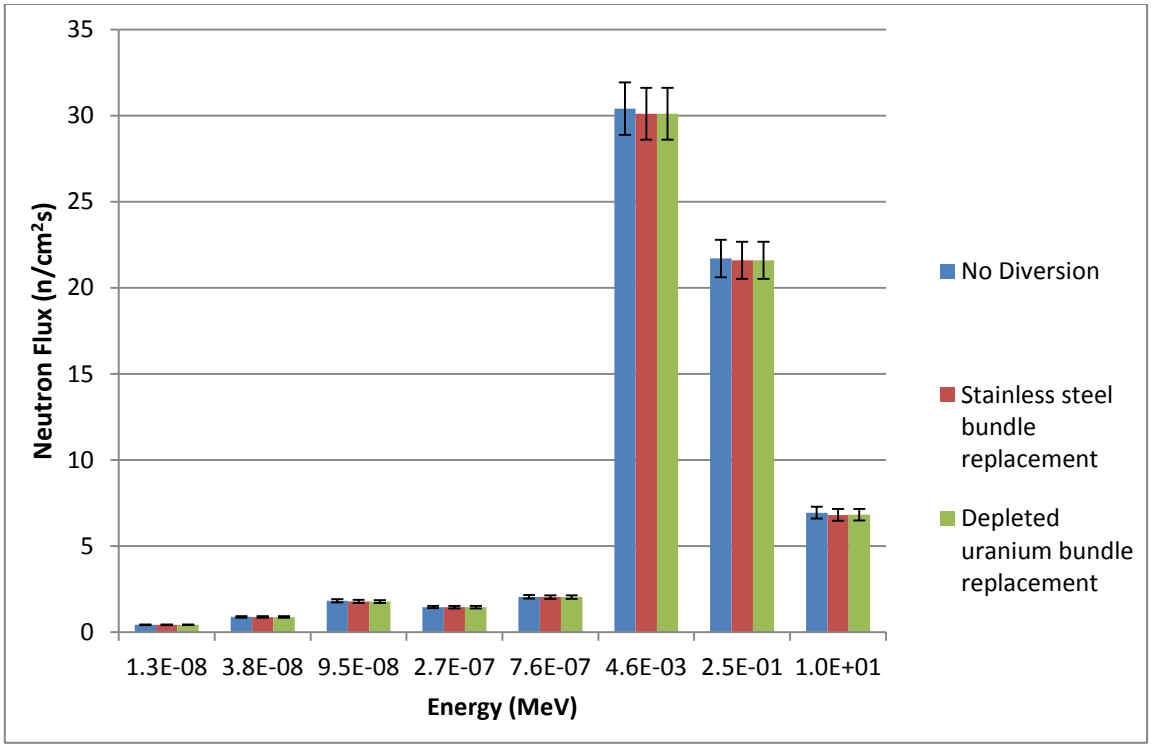

Fig. 31: Schematic representation of variation of neutron flux for no diversion case and diversion cases with dummy stainless steel and depleted uranium dioxide bundles replacement.

From the Fig. 31 and Table IX, it can be inferred that the change in neutron fluxes between no diversion case and diversion cases (9 spent fuel bundles from the region opposite to the collimator) (refer Fig. 30) is very small (practically no difference).

The obtained flux at the ^{3}He detector inside the re-verification tube was converted to $^{3}He(n,p)^{3}H$ reaction rates. The calculated reaction rates are given in Table X. Results shown in Table X also suggest that there is no significant difference in reaction rates between no diversion case and diversion cases.

TABLE X

$^{3}He(n,p)^{3}H$ reaction rates at the detector inside re-verification tube.

Diversion Case	**$^{3}He(n,p)^{3}H$ reaction rate (per second) in ^{3}He tube**
No Diversion	18.0
9 bundles diversion with DU replacement	17.8
9 bundles diversion with SS replacement	17.8

V.B. Sensitivity of the Detection System with respect to the Removal of the Spent Fuel Bundles from the Basket

MCNP models were developed to determine the sensitivity of the detection system with respect to the removal of the spent fuel bundles from the basket and replacing it by dummy bundles made of depleted uranium dioxide bundles. Eight additional diversion cases were considered along with no diversion case, where in each case 3 additional spent fuel bundles were removed and replaced by the dummy depleted uranium dioxide bundles. Fig. 32 shows the images of the models used to determine the sensitivity of the detection system with respect to the removal of spent fuel bundles.

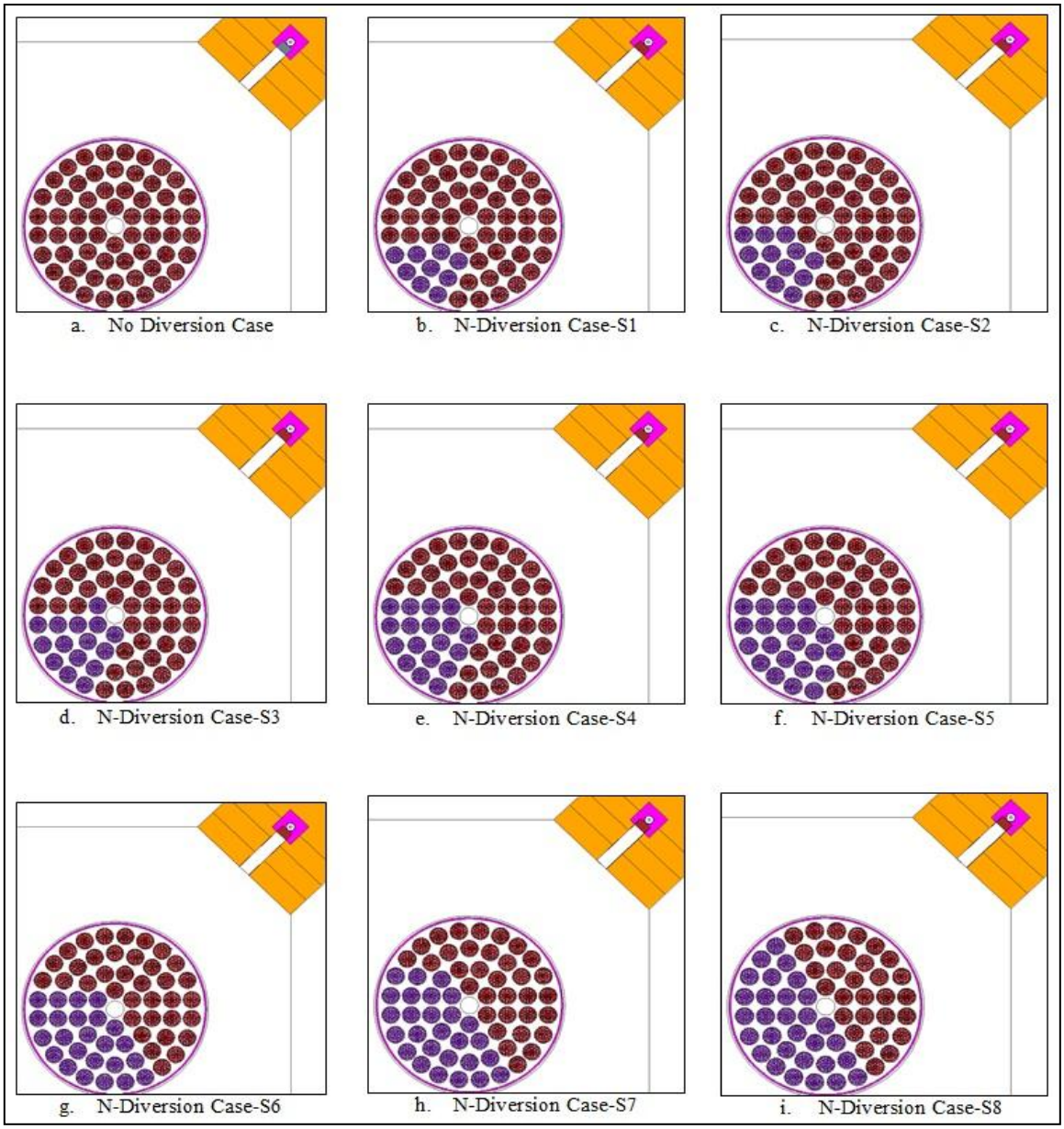

Fig. 32: Images of the models used to determine the sensitivity of the detection system with respect to the removal of spent fuel bundles.

The comparison of energy dependent neutron group fluxes obtained at the detector inside the re-verification tube for the no diversion case and other 8 diversion cases with 2” polyethylene inside the collimator at detector end are given in Table XI. The MCNP

estimated percent error for all the cases were almost same and are given in last column of Table XI.

TABLE XI

Neutron flux estimated at the detector inside re-verification tube for no diversion case and 8 various diversion cases with 2-inch polyethylene at detector end inside the collimator.

Neutron Energy Group (MeV)	**Neutron Flux (n/cm^2-s)**				
	No Diversion	**N-Diversion case-S1**	**N-Diversion case-S2**	**N-Diversion case-S3**	**N-Diversion case-S4**
1.0E-9 to 2.5E-8	4.32E-1	4.34E-1	4.24E-1	4.23E-1	4.49E-1
2.5E-8 to 5.0E-8	8.88E-1	8.78E-1	8.71E-1	8.33E-1	8.57E-1
5.0E-8 to 1.4E-7	1.82E+0	1.78E+0	1.81E+0	1.77E+0	1.86E+0
1.4E-7 to 4.0E-7	1.46E+0	1.45E+0	1.48E+0	1.43E+0	1.41E+0
4.0E-7 to 1.1E-6	2.05E+0	2.04E+0	2.00E+0	1.99E+0	2.04E+0
1.1E-6 to 9.1E-3	3.04E+1	3.01E+1	3.03E+1	3.05E+1	3.06E+1
9.1E-3 to 5.0E-1	2.17E+1	2.16E+1	2.20E+1	2.17E+1	2.18E+1
5.0E-1 to 2.0E+1	6.94E+0	6.82E+0	6.75E+0	7.09E+0	6.93E+0
Total	6.57E+1	6.51E+1	6.56E+1	6.57E+1	6.60E+1

Neutron Energy Group (MeV)	**Neutron Flux (n/cm^2-s)**				
	N-Diversion case-S5	**N-Diversion case-S6**	**N-Diversion case-S7**	**N-Diversion case-S8**	**% Statistical Error**
1.0E-9 to 2.5E-8	4.10E-1	4.47E-1	4.26E-1	4.41E-1	3.57
2.5E-8 to 5.0E-8	8.51E-1	8.55E-1	9.26E-1	8.49E-1	2.65
5.0E-8 to 1.4E-7	1.76E+0	1.75E+0	1.79E+0	1.82E+0	1.93
1.4E-7 to 4.0E-7	1.40E+0	1.38E+0	1.50E+0	1.45E+0	2.18
4.0E-7 to 1.1E-6	1.97E+0	1.92E+0	2.06E+0	2.03E+0	1.98
1.1E-6 to 9.1E-3	3.02E+1	3.00E+1	3.01E+1	3.01E+1	0.72
9.1E-3 to 5.0E-1	2.15E+1	2.14E+1	2.14E+1	2.13E+1	0.92
5.0E-1 to 2.0E+1	6.69E+0	6.93E+0	6.85E+0	6.89E+0	1.68
Total	6.48E+1	6.46E+1	6.50E+1	6.49E+1	0.52

The variation neutron fluxes with respect to neutron energy are schematically shown in Fig. 33.

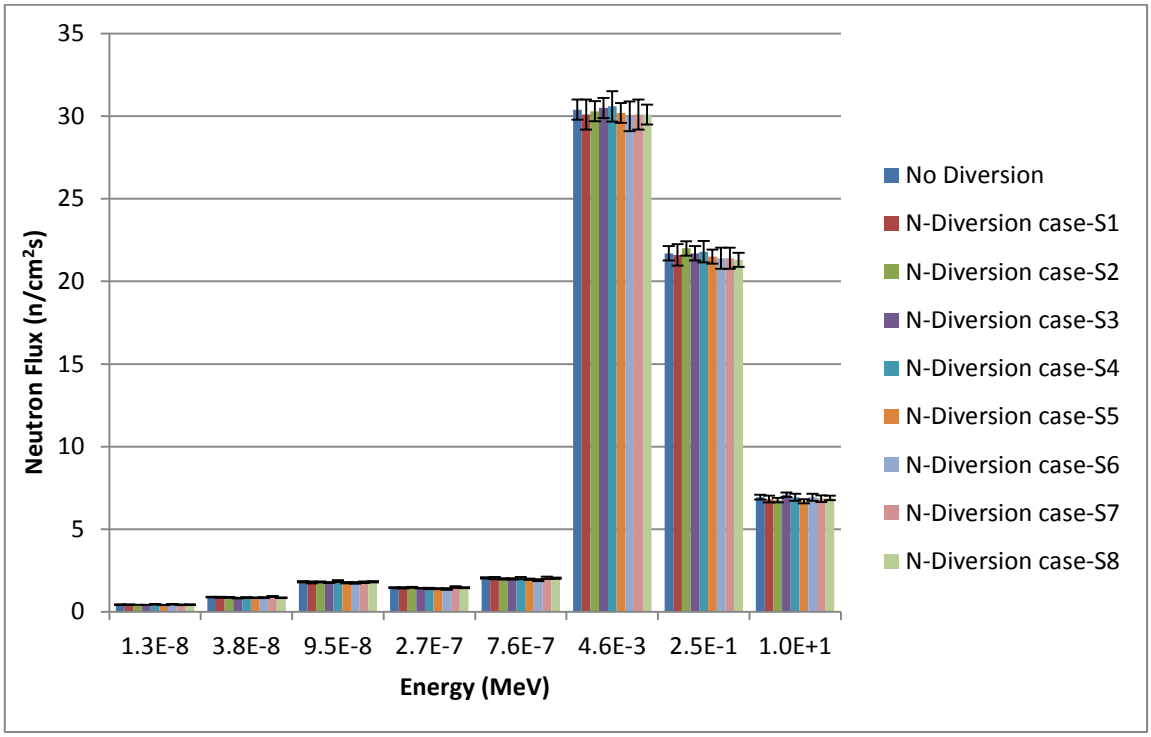

Fig. 33: Schematic representation of variation of neutron flux for no diversion case and 8 various diversion cases used to determine the sensitivity of the detection system.

The ^{3}He reaction rate was estimated by MCNP simulation for no diversion case and different diversion scenarios. The comparison of the ^{3}He reaction rate inside the detector for all the cases is given in Table XII.

TABLE XII

^{3}He reaction rate for no diversion case and different diversion cases.

Case	Scenario	Reaction rate (Rxn/s)
No Diversion	No Diversion	17.97
N-Diversion case-S1	9 Bundles removed & replaced by depleted U bundles	17.76
N-Diversion case-S2	12 Bundles removed & replaced by depleted U bundles	17.73
N-Diversion case-S3	15 Bundles removed & replaced by depleted U bundles	17.62
N-Diversion case-S4	18 Bundles removed & replaced by depleted U bundles	17.95
N-Diversion case-S5	21 Bundles removed & replaced by depleted U bundles	17.38
N-Diversion case-S6	24 Bundles removed & replaced by depleted U bundles	17.47
N-Diversion case-S7	27 Bundles removed & replaced by depleted U bundles	17.94
N-Diversion case-S8	30 Bundles removed & replaced by depleted U bundles	17.84

From the Tables XI and XII and Fig. 30, it can be inferred that there is no significant neutron signal reduction even when 30 spent fuel bundles are removed from a basket region on the opposite side of the collimator (refer image in Fig. 32).

V.C. Inverse MCNP model

An inverse MCNP model was developed to determine which of the bundles in the basket were contributing to the total neutron flux obtained in the detector. In this model, neutrons were generated at the position of ^{3}He detector inside the re-verification tube in

line with the collimator and spent fuel storage basket. The transported neutrons were collected at the 60 positions inside the spent fuel storage basket, which are the positions of 60 fuel bundles inside the storage basket.

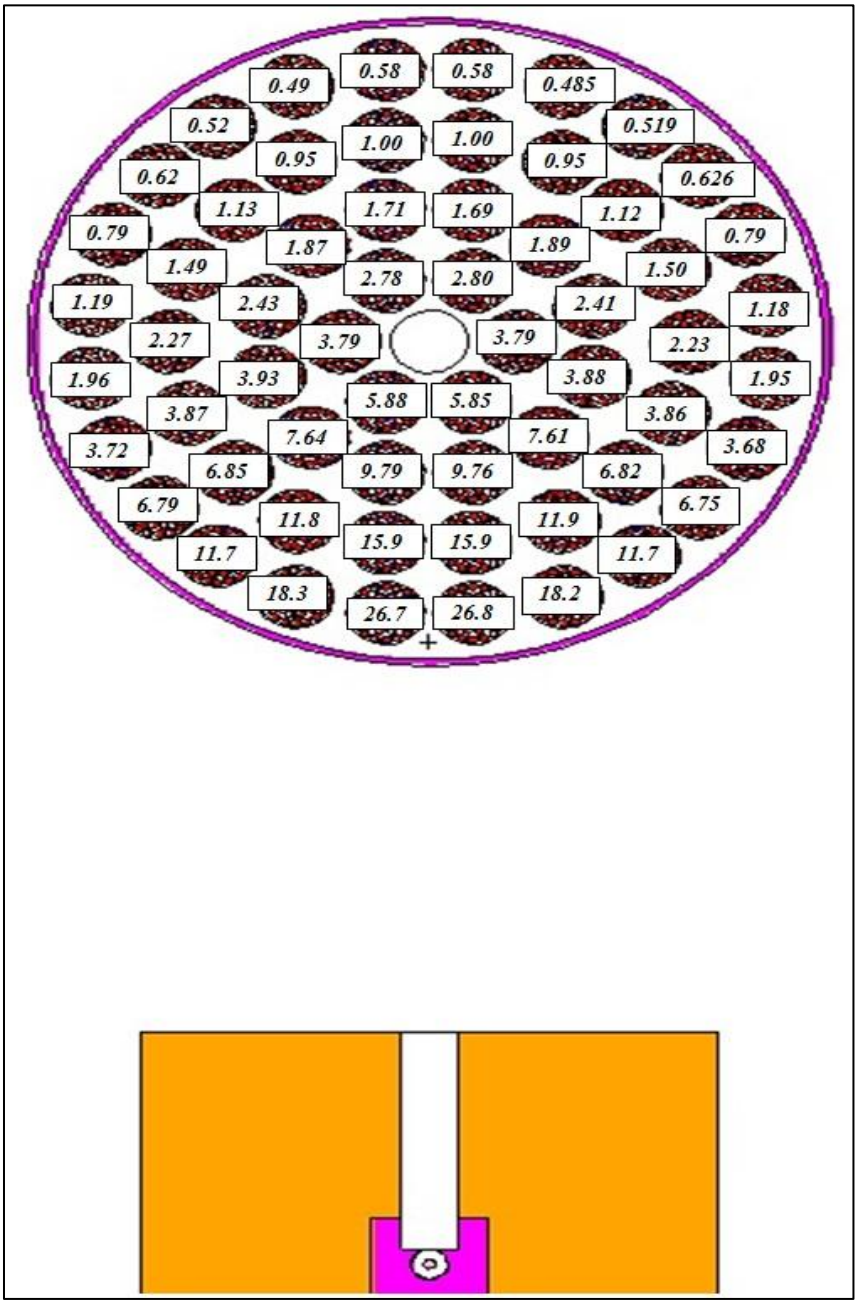

Fig. 34: Neutron flux at 60 different positions in the inverse model.

This model gave a better understanding of the scenario, from this inverse simulation, it is inferred that the neutron flux contribution from almost 40 spent fuel bundles in the region of the basket which is opposite to detector was relatively small (negligible), as shown in Fig. 34. Numbers shown in the Fig. 34 on each bundle are total neutron flux (n/cm^2-s) at that position.

From this observation, it can be concluded that it will be very difficult to determine the diversion of about 40 spent fuel bundles (~67% of bundles in a basket) from the storage basket region opposite to the collimator and re-verification tube.

V.D. Vertical Neutron Profile

The vertical neutron profile response of the detecting system of the MACSTOR KN-400 was studied by modifying the MCNP models. Ten ^{3}He detectors were placed inside the central re-verification tube in line with the collimators facing the spent fuel storage baskets in a silo (refer Fig. 19). MCNP neutron simulation was performed by starting the source particles from all the spent fuel bundles in 40 storage baskets around the central re-verification tube. For the diversion case, all 60 spent fuel bundles were removed from one of the baskets and replaced by the dummy bundles made of depleted uranium.

The comparison of the total, thermal and fast neutron fluxes obtained at each detector inside the re-verification tube for no diversion case is given in Table XIII and for diversion case is given in Table XIV. The variation of total neutron flux with respect to detectors from bottom to top for both no diversion and diversion case is schematically shown in Fig. 35.

TABLE XIII

Comparison of neutron fluxes at each detector inside the re-verification tube for no diversion case.

Detector	Neutron Flux (n/cm^2-s)			
	No Diversion Case			
	Thermal	Fast	Total	% Statistical Error
1 (Bottom)	1.11E+00	1.15E+01	1.26E+01	1.21
2	1.49E+00	1.53E+01	1.68E+01	1.01
3	1.53E+00	1.62E+01	1.78E+01	0.99
4	1.56E+00	1.60E+01	1.76E+01	0.96
5	1.60E+00	1.61E+01	1.77E+01	1.02
6	1.54E+00	1.59E+01	1.75E+01	0.98
7	1.61E+00	1.62E+01	1.79E+01	0.99
8	1.58E+00	1.61E+01	1.76E+01	0.98
9	1.56E+00	1.56E+01	1.72E+01	1.13
10 (top)	1.23E+00	1.27E+01	1.39E+01	1.13

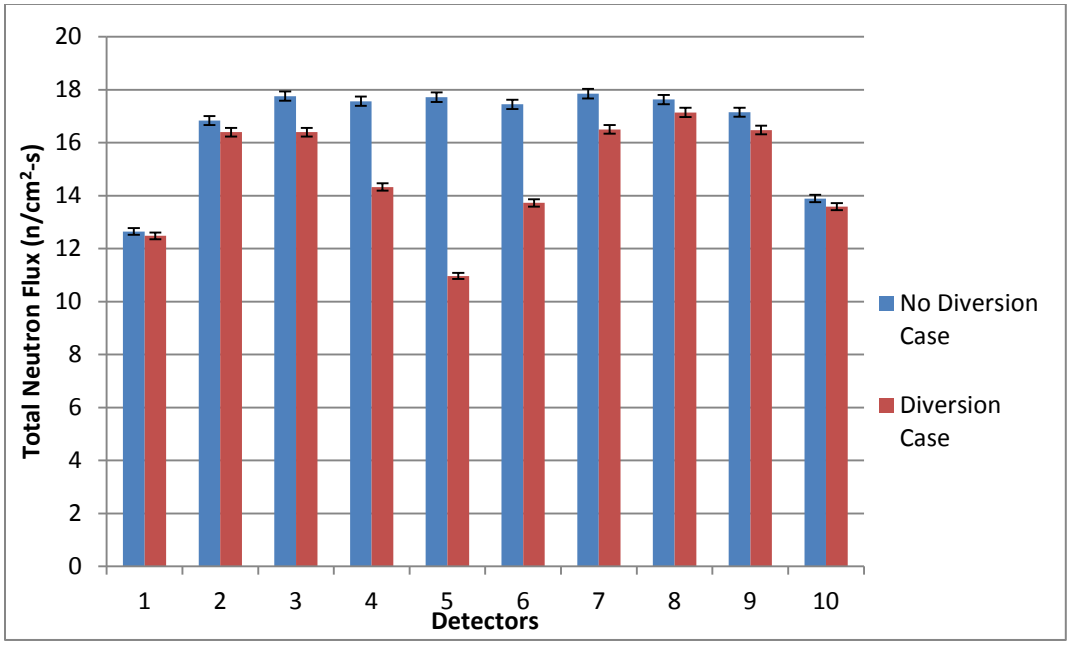

Fig. 35: Schematic representation of the variation of total neutron flux collected at all 10 detectors inside central re-verification tube.

TABLE XIV

Comparison of neutron fluxes at each detector inside the re-verification tube for diversion case.

Detector	Neutron Flux (n/cm^2-s)			
	Diversion Case			
	Thermal	Fast	Total	% Statistical Error
1 (Bottom)	1.09E+00	1.14E+01	1.25E+01	1.17
2	1.46E+00	1.49E+01	1.64E+01	0.99
3	1.49E+00	1.49E+01	1.64E+01	0.98
4	1.23E+00	1.31E+01	1.43E+01	1.09
5	1.01E+00	9.96E+00	1.10E+01	1.19
6	1.20E+00	1.25E+01	1.37E+01	1.07
7	1.42E+00	1.51E+01	1.65E+01	0.98
8	1.54E+00	1.56E+01	1.71E+01	0.95
9	1.43E+00	1.51E+01	1.65E+01	0.98
10 (top)	1.23E+00	1.24E+01	1.36E+01	1.08

All 60 spent fuel bundles were removed from a storage basket in line with the 5th detector for the diversion case. From the Tables XIII, XIV and Fig. 35, it can be inferred that the 5th detector in line with the diverted basket gave a total neutron signal reduction by a factor of ~1.2.

V.E. Diversion Analysis Using Peripheral Structure of the MACSTOR KN-400 Facility

For the diversion analysis using the peripheral structure of the MACSTOR KN-400 facility, ten ^{3}He detectors were placed inside the peripheral re-verification tube in line with each spent fuel storage basket in a silo. MCNP neutron simulations were performed

by starting the source particles from the adjacent silos (refer Fig. 22) and the particles were collected in all 10 detectors inside the peripheral re-verification tube.

For the diversion case, all 60 spent fuel bundles were removed and replaced by the depleted uranium dioxide dummy bundles from one of the spent fuel storage baskets in a silo (refer Fig. 22).

The comparison of the total, thermal and fast neutron fluxes obtained at each detector inside the peripheral re-verification tube for all cases are provided in Table XV. The variation of total neutron flux with respect to detectors from bottom to top for both no diversion and diversion case is schematically shown in Fig. 36.

TABLE XV

Comparison of neutron fluxes for no diversion and diversion case for peripheral structure

Detector	**Neutron Flux (n/cm^2-s)**					
	No Diversion Case			**Diversion Case**		
	Total	**Thermal**	**Fast**	**Total**	**Thermal**	**Fast**
1 (Bottom)	3.21E+2	4.96E+0	3.16E+2	3.14E+2	4.61E+0	3.10E+2
2	4.84E+2	7.67E+0	4.77E+2	4.69E+2	7.44E+0	4.61E+2
3	5.47E+2	9.03E+0	5.38E+2	5.12E+2	8.42E+0	5.04E+2
4	5.76E+2	9.59E+0	5.66E+2	4.77E+2	8.11E+0	4.69E+2
5	5.88E+2	9.66E+0	5.79E+2	4.17E+2	7.34E+0	4.10E+2
6	5.91E+2	9.77E+0	5.82E+2	4.83E+2	8.07E+0	4.75E+2
7	5.78E+2	9.45E+0	5.69E+2	5.41E+2	8.76E+0	5.32E+2
8	5.51E+2	9.09E+0	5.42E+2	5.36E+2	8.95E+0	5.28E+2
9	4.82E+2	7.97E+0	4.74E+2	4.77E+2	7.80E+0	4.70E+2
10 (Top)	3.27E+2	4.97E+0	3.22E+2	3.24E+2	5.16E+0	3.19E+2

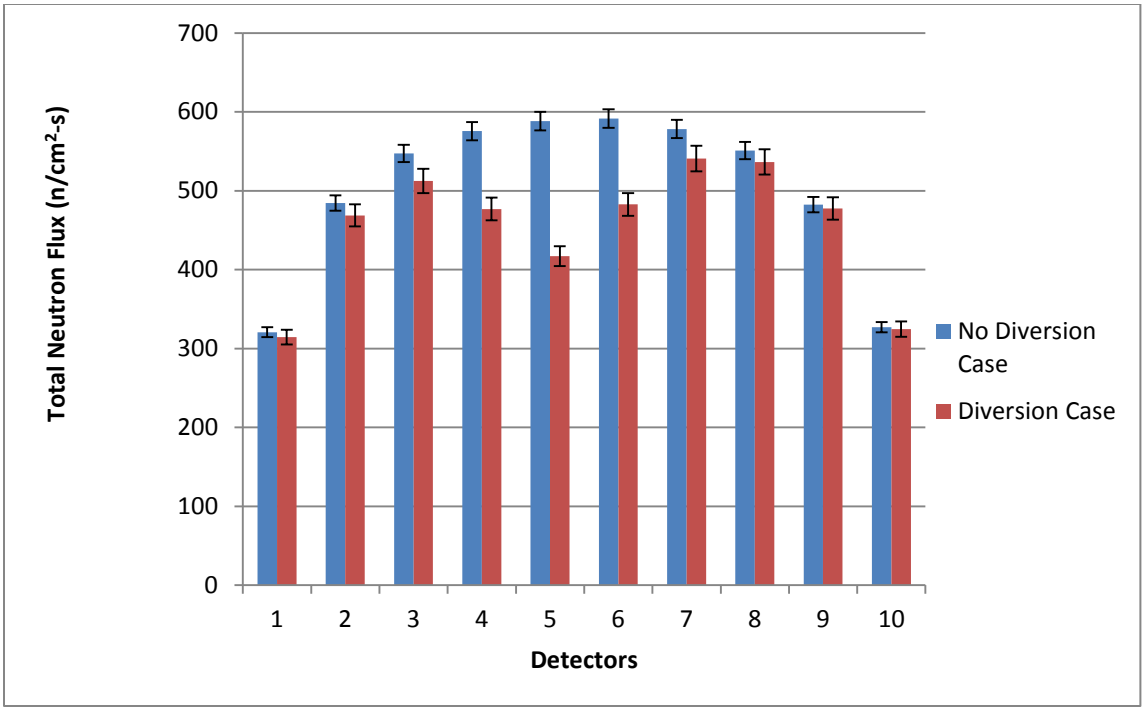

Fig. 36: Schematic representation of variation of total neutron flux collected at all 10 detectors inside peripheral re-verification tube.

TABLE XVI

^{3}He reaction rate in all 10 detectors inside the peripheral re-verification tube for both no diversion and diversion case.

Detector	**^{3}He Reaction rate (Rxn/s)**	
	No Diversion case	**Diversion Case**
1 (Bottom)	34.5	33.0
2	53.7	52.1
3	62.3	57.7
4	66.8	56.2
5	68.2	51.7
6	69.3	57.0
7	66.3	62.1
8	63.6	61.5
9	54.5	53.4
10 (Top)	35.1	35.6

The ^{3}He reaction rate was also estimated by the MCNP simulation and the obtained results are given in Table XVI. All 60 spent fuel bundles were removed from a storage basket in line with the 5th detector for diversion cases. From the Fig. 36, Tables XV and XVI, it can be observed that the detector 5 in line with the diverted spent fuel storage basket gave a total neutron signal reduction by a factor of ~1.5.

V.F. Non-Detection Probability

From the previous calculations (refer Chapter 2), it is required to divert ~140 spent fuel bundles from the facility to get 1 SQ of Pu. The MCNP model was developed to estimate the non-detection probability for the neutron measurement. In the model, 14 spent fuel bundles from each of the baskets in a silo, which sum up to 140 spent fuel bundles (1 SQ of Pu material) was removed and replaced by depleted uranium dioxide as shown in Fig. 37.

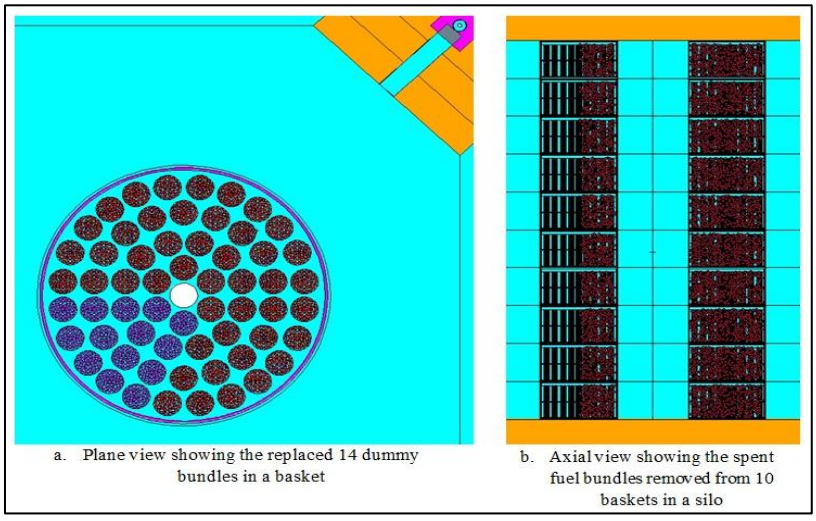

Fig. 37: Views of the model showing the replaced 14 dummy depleted uranium dioxide bundles in each of the baskets in a silo

Ten ^{3}He detectors were placed inside the re-verification tube in line with the collimators facing the storage baskets in a silo. The obtained total neutron fluxes in each detector for no diversion and diversion case are tabulated in Table XVII and Table XVIII respectively. The pictorial representation of the variation of the total neutron flux for both the cases is shown in Fig. 38.

TABLE XVII

Neutron flux obtained for no diversion case used to estimate non-detection probability

Detector	**Neutron Flux (n/cm^2-s)**			
	Thermal	**Fast**	**Total**	**% Statistical Error**
1 (Bottom)	3.17E+00	4.13E+01	4.45E+01	1.94
2	4.21E+00	5.65E+01	6.07E+01	1.83
3	4.03E+00	5.76E+01	6.16E+01	1.82
4	4.50E+00	6.03E+01	6.48E+01	1.82
5	4.47E+00	5.96E+01	6.41E+01	1.80
6	4.60E+00	5.91E+01	6.37E+01	2.15
7	4.65E+00	6.10E+01	6.56E+01	1.91
8	4.77E+00	5.97E+01	6.45E+01	1.93
9	4.23E+00	5.70E+01	6.12E+01	1.89
10 (Top)	3.35E+00	4.54E+01	4.87E+01	2.24

TABLE XVIII

Neutron flux obtained for diversion case used to estimate non-detection probability

Detector	Neutron Flux (n/cm^2-s)			
	Thermal	Fast	Total	% Statistical Error
1 (Bottom)	3.07E+00	4.23E+01	4.54E+01	1.49
2	3.94E+00	5.41E+01	5.81E+01	1.41
3	4.54E+00	5.83E+01	6.28E+01	1.42
4	4.42E+00	5.91E+01	6.35E+01	1.43
5	4.51E+00	5.98E+01	6.43E+01	1.44
6	4.64E+00	5.86E+01	6.33E+01	1.66
7	4.54E+00	5.87E+01	6.33E+01	1.42
8	4.20E+00	5.70E+01	6.12E+01	1.44
9	4.17E+00	5.67E+01	6.08E+01	1.45
10 (top)	3.29E+00	4.49E+01	4.82E+01	1.72

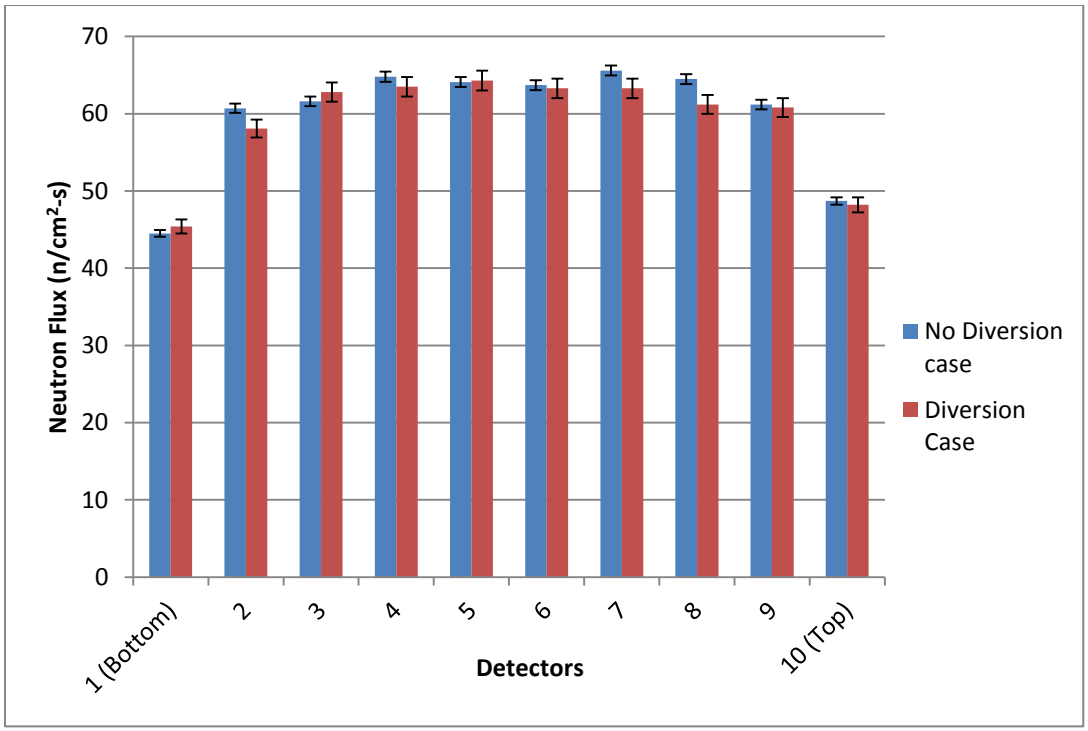

Fig. 38: Variation of total neutron flux for no diversion and diversion case used to estimate the non-detection probability

From Tables XVII, XVIII and Fig. 38, it can be observed that there is very small signal difference (practically no signal difference) between no diversion case and diversion. The non-detection probability calculated using the obtained data was almost equal to 1. By this simulation, it can be concluded that 1 SQ of Pu (140 spent fuel bundles) material can be easily diverted if the diverting state or organization is smart enough to divert 14 spent fuel bundles from each of the baskets in a silo, from the basket region opposite to the collimator of the re-verification tube. This confirms that the non-detection probability of the current detection system is 1 for specific cases as observed by the simulations.

Similar MCNP simulations were performed to estimate the non-detection probability of the current detection system with respect to the diversion of spent fuel bundles from the storage baskets in a silo. In this simulation, eight scenarios were considered; in each scenario spent fuel bundles from an additional basket were diverted, such that, in each case ~140 spent fuel bundles were diverted from a silo. By using the simulation results, non-detection probability (β_{tot}) and detection probability (P_D) of the detection system for each case were estimated. The scheme of the diversions and the results obtained are given in Table XIX.

TABLE XIX

Scheme of diversions, non-detection and detection probability.

Baskets	Scenario 1		Scenario 2		Scenario 3		Scenario 4	
	No. of bundles	β	No. of bundles	β	No. of bundles	β	No. of bundles	β
1	60	0.001	35	0.897	28	0.957	24	0.969
2	60	0.001	35	0.897	28	0.957	24	0.969
3	21	0.982	35	0.897	28	0.957	24	0.969
4			35	0.897	28	0.957	24	0.969
5					28	0.957	24	0.969
6							24	0.969
β_{tot}		0.000		0.646		0.803		0.830
P_D		1.000		0.354		0.197		0.170
Baskets	**Scenario 5**		**Scenario 6**		**Scenario 7**		**Scenario 8**	
	No. of bundles	**β**	**No. of bundles**	**β**	**No. of bundles**	**β**	**No. of bundles**	**β**
1	20	0.982	17	0.988	16	0.990	14	0.991
2	20	0.982	17	0.988	16	0.990	14	0.991
3	20	0.982	17	0.988	16	0.990	14	0.991
4	20	0.982	17	0.988	16	0.990	14	0.991
5	20	0.982	18	0.988	16	0.990	14	0.991
6	20	0.982	18	0.988	15	0.990	14	0.991
7	20	0.982	18	0.988	15	0.990	14	0.991
8			18	0.988	15	0.990	14	0.991
9					15	0.990	14	0.991
10							14	0.991
β_{tot}		0.882		0.905		0.914		0.915
P_D		0.118		0.095		0.086		0.085

The results obtained for non-detection probability is pictorially shown in Fig. 39. The detection probability of the detection system is pictorially shown in Fig. 40.

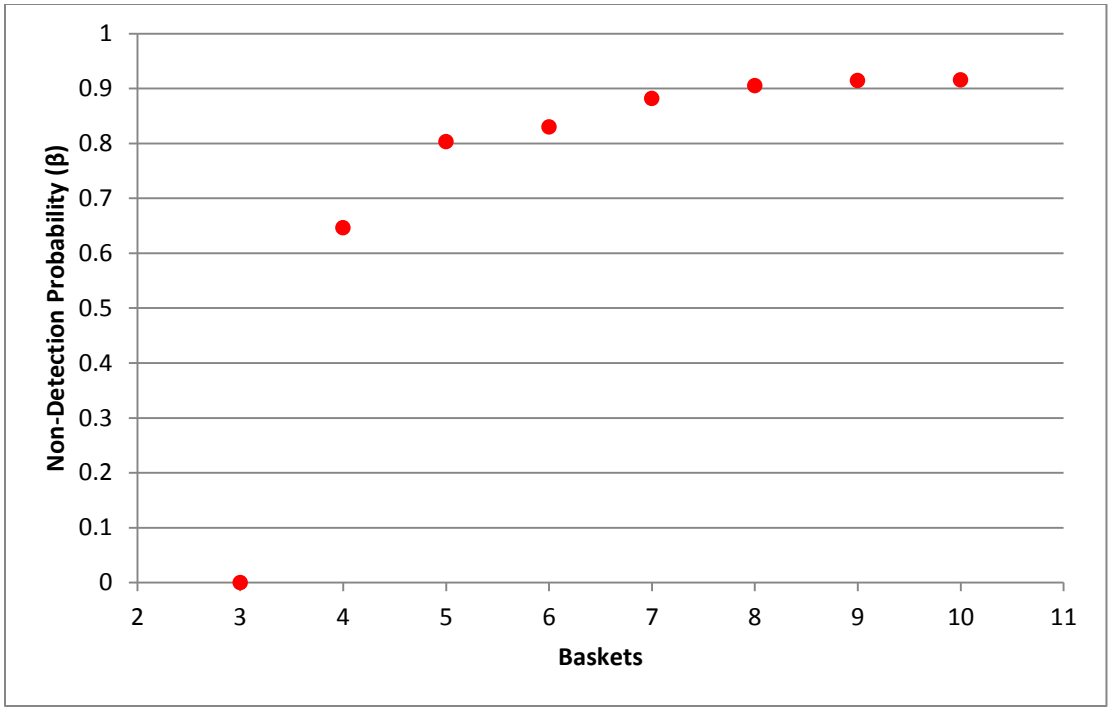

Fig. 39: Non-detection probability of the detection system with respect to diversion from the storage baskets.

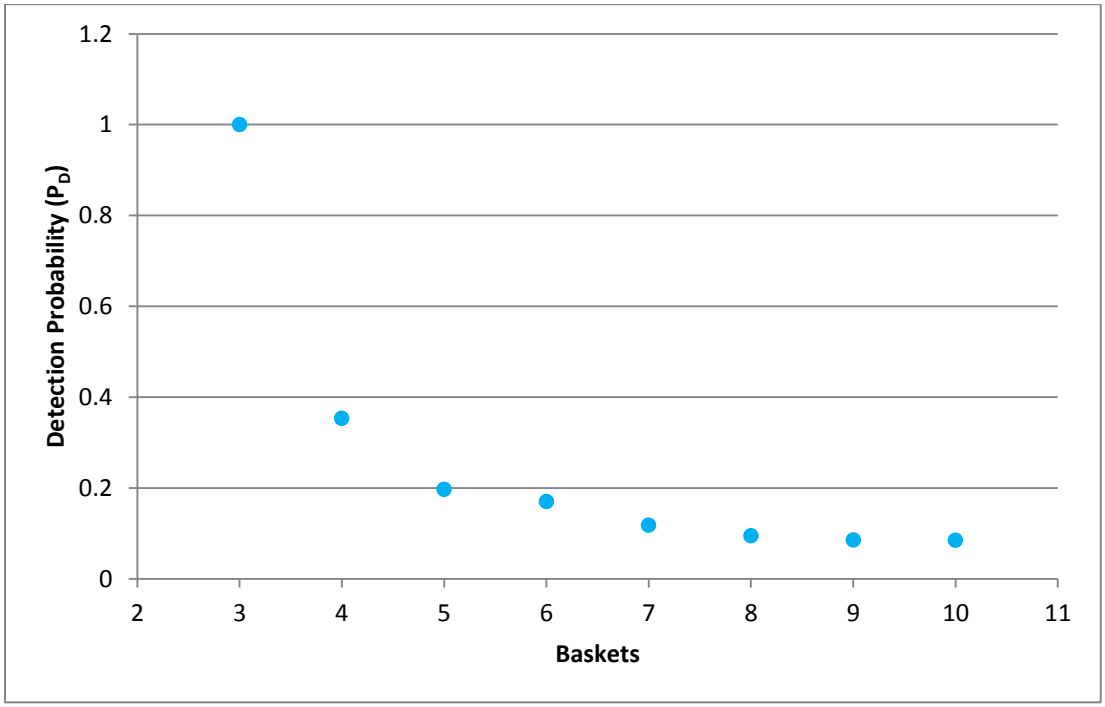

Fig. 40: Detection probability of the detection system with respect to diversion from the storage baskets.

CHAPTER VI

SUMMARY AND CONCLUSIONS

This study focused on the evaluation of the gamma and neutron fingerprinting method for spent fuel verification in the MACSTOR KN-400 CANDU dry storage facility. The gamma and neutron source strength of CANDU6 spent fuel was estimated using ORIGEN-ARP burnup code. An MCNP model of a 37-fuel pins CANDU6 fuel bundle was developed. The MCNP model was further expanded to develop a spent fuel storage basket containing 60 spent fuel bundles. An MCNP model of a silo, which can hold up to 10 spent fuel storage baskets, was developed. The MCNP model of the central structure of the MACSTOR KN-400 facility, which contains four silos with the central re-verification tube along with carbon steel and high density concrete shield, was developed. The MCNP model of the peripheral structure of the MACSTOR KN-400 facility, which contains peripheral re-verification tube running through the module wall for a silo, was also developed.

MCNP gamma and neutron simulations were performed using both central and peripheral structure of MACSTOR KN-400. CZT and ^{3}He detectors were placed inside the re-verification tube in line with the spent fuel storage basket to measure the gamma and neutron flux respectively. The sensitivity of the measurement system was tested by considering various diversion scenarios. In the diversion cases, the spent fuel bundles from the storage basket were replaced by stainless steel or depleted uranium dioxide dummy bundles.

Gamma transport simulation studies suggested that the detection of spent fuel diversion is difficult if only the gamma signals at the re-verification tube are considered. This is because the gamma signals reaching the detector inside the re-verification tube are essentially from the spent fuel bundles that are stored in the peripheral region of the basket which faces the collimator of the re-verification tube. So, if the diversion occurs from the internal regions of the basket, the gamma signal decrease cannot be measured and it will be very difficult to detect spent fuel bundles diversion. However, the vertical profile of the gamma radiation showed that it could be effective in monitoring the constant signal level from the spent fuel when COK is not lost.

Neutron transport simulation studies suggests that there are changes in neutron signals, especially the fast neutron signals reaching the detector inside the re-verification tube when the spent fuel bundles are removed from the region of the storage basket facing the collimator of the re-verification tube. Also, it is found from the neutron transport simulations that the probability of detection of diversion of about 40 spent fuel bundles from the basket region opposite (which is not seeing the collimator of the re-verification tube) to the collimator is very low. Diversion of any of these 40 spent fuel bundles is difficult to detect. However, it should be noted here that to obtain 1 SQ of plutonium at least 138 spent fuel bundles are required to be diverted. Therefore, an adversary could attempt to divert 47 spent fuel bundles from each of the three baskets to acquire 1 SQ. This kind of diversion reduces the neutron signal significantly at the detector. The probability of detecting this diversion is almost equal to 1.

By introducing thermalizing material between the detector and the spent fuel storage basket the sensitivity of the detection system to the diversion of the spent fuel bundles from the storage basket is improved by a factor of 3.

Non-detection probability for removing ~140 spent fuel bundles as a function of number of baskets is also determined. In the worst scenario, the diverting state or organization could divert 14 spent fuel bundles from each of 10 baskets in a silo from the basket region opposite to the collimator of the re-verification tube. The non-detection probability for this scenario is close to 1. This diversion cannot be easily detected using the currently designed detection system. In order to increase the detection probability, either the design of the facility must be changed or other safeguard methods, such as containment and surveillance methods must be used for safeguarding the nuclear material at the facility.

REFERENCES

1. S. S. PARK, J. S. SHIN, and J. K. YEO, "Safeguards Approach to the MACSTOR KN-400 Type Dry Storage at the Wolsung Facility," A report by Korea Institute of Nuclear Non-proliferation and Control (2006).
2. C. JAMES, M. GAMIL, and C SANDRA, "Design Description for Reverification System," KN-N-AE-D-G-001, Korea Hydro & Nuclear Power Co., Ltd (Dec. 2006).
3. I.C. GAULD, S.M. BOWMAN, and J.E. HORWEDEL, "ORIGEN-ARP: Automatic Rapid Processing for Spent Fuel Depletion, Decay, and Source Term Analysis," ORNL/TM-2005/39, Oak Ridge National Laboratory (Jan. 2009).
4. X-5 MONTE CARLO TEAM, "MCNP - A General Monte Carlo N-Particle Transport Code," Version 5, Vol. 1 & 2, Los Alamos National Laboratory (April 2003).
5. K. D. KOK, *Nuclear Engineering Handbook*, CRC Press (June 2009).
6. CANDU6 PROGRAM TEAM, "CANDU6 Technical Summary," Reactor Development Business Unit, Atomic Energy of Canada Limited (AECL) (June 2005); available at http://www.scribd.com/doc/39973366/C6-Technical-Summary.

7. M. BUNN, J. P. HOLDREN, A. MACFARLANE, S. E. PICKETT, A. SUZUKI, T. SUZUKI and J. WEEKS, "Interim Storage of Spent Nuclear Fuel: A Safe, Flexible, and Cost-Effective Near-Term Approach to Spent Fuel Management," Harvard University and University of Tokyo (June 2001); available at http://www.whrc.org/resources/publications/pdf/BunnetalHarvardTokyo.01.pdf
8. NUCLEAR WASTE MANAGEMENT DIVISION ONTARIO POWER GENERATION INC., "Nuclear Waste Management: Technical Support Document," New Nuclear-Darlington Environmental Assessment (Aug. 2009); available at http://www.ceaa.gc.ca/050/documents_staticpost/cearref_29525/0104/nwm.pdf
9. INTERNATIONAL ATOMIC ENERGY AGENCY, "Good Practices in Heavy Water Reactor Operation," IAEA-TECDOC-1650, International Atomic Energy Agency, Vienna (2010); available at http://www-pub.iaea.org/MTCD/publications/PDF/te_1650_web.pdf
10. K. D. VEAL, M. E. ABHOLD, and H. O. MENLOVE, "Verification of CANDU Spent Fuel in Sealed Storage Casks," LA-UR-00-2794, Los Alomos National Laboratory (July 2000).
11. INTERNATIONAL ATOMIC ENERGY AGENCY, "IAEA Safeguards Glossary, International Nuclear Verification Series No. 3," IAEA/NVS/3, International Atomic Energy Agency, Vienna (2002); available at http://www-pub.iaea.org/MTCD/publications/PDF/nvs-3-cd/PDF/NVS3_prn.pdf

12. A. B. CHILTON, J. K. SHULTIS, and R. E. FAW, *Principles of Radiation Shielding*, Prentice-Hall (1984).

13. C. GRUPEN and I. BUVAT (eds.), *Handbook of Particle Detection and Imaging*, DOI 10.1007/978-3-642-13271-1_1, © Springer-Verlag Berlin Heidelberg (2012).

14. LND, INC., "Cylindrical He3 Neutron Detector"; available at http://lndinc.com/products/536/. (*Last accessed: April 2012*)

15. R. G. WILLIAMS III, C. J. GESH, R. T. PAGH, "Compendium of Material Composition Data for Radiation Transport Modeling," PNNL-15870, Pacific Northwest National Laboratory (April 2006); available at http://www.pnl.gov/main/publications/external/technical_reports/PNNL-15870.pdf

APPENDIX A

Table XX: Gamma energy group and respective source strength.

Energy (MeV)	Photon Source Strength (γ/s)	Energy (MeV)	Photon Source Strength (γ /s)	Energy (MeV)	Photon Source Strength (γ /s)	Energy (MeV)	Photon Source Strength (γ /s)
0.00E+00	0.00E+00	6.82E-02	7.01E+10	5.58E-01	5.12E+08	7.95E-01	4.72E+09
9.00E-04	0.00E+00	7.00E-02	1.02E+11	5.63E-01	3.59E+10	7.96E-01	9.67E+08
9.20E-04	7.98E+10	8.60E-02	4.94E+11	5.64E-01	2.72E+10	8.45E-01	1.05E+10
7.00E-03	0.00E+00	8.62E-02	1.54E+08	5.69E-01	3.59E+10	8.46E-01	1.12E+09
7.20E-03	4.95E+09	8.65E-02	9.26E+09	5.70E-01	5.01E+10	8.50E-01	1.45E+09
8.50E-03	0.00E+00	8.67E-02	3.16E+10	5.82E-01	8.62E+10	8.51E-01	4.55E+08
8.70E-03	2.24E+11	1.00E-01	4.10E+11	5.83E-01	1.69E+09	8.73E-01	7.99E+09
9.20E-03	0.00E+00	1.01E-01	5.12E+10	5.91E-01	5.74E+10	8.74E-01	2.31E+10
9.40E-03	2.46E+10	1.05E-01	5.46E+10	5.92E-01	9.40E+09	8.92E-01	6.53E+09
1.02E-02	0.00E+00	1.06E-01	2.10E+10	6.04E-01	8.62E+10	8.93E-01	9.67E+08
1.06E-02	1.16E+08	1.23E-01	2.32E+11	6.05E-01	3.17E+11	9.04E-01	3.99E+09
1.10E-02	0.00E+00	1.24E-01	8.72E+10	6.25E-01	1.44E+11	9.05E-01	1.69E+09
1.14E-02	3.05E+09	1.27E-01	4.10E+10	6.26E-01	6.07E+08	9.96E-01	3.30E+10
2.00E-02	8.05E+12	1.28E-01	4.12E+10	6.61E-01	2.51E+11	9.97E-01	2.00E+10
2.64E-02	1.19E+12	1.50E-01	3.01E+11	6.62E-01	1.22E+13	1.00E+00	1.09E+09
2.66E-02	3.27E+08	1.88E-01	2.03E+11	6.76E-01	1.01E+11	1.00E+00	1.22E+08
2.74E-02	1.49E+11	1.89E-01	4.55E+08	6.77E-01	3.03E+08	1.01E+00	3.40E+10
2.76E-02	1.71E+09	2.47E-01	3.10E+11	6.92E-01	1.08E+11	1.04E+00	1.01E+09
2.86E-02	1.86E+11	2.48E-01	1.31E+10	6.93E-01	3.39E+09	1.04E+00	3.25E+09
2.88E-02	2.09E+09	3.00E-01	2.78E+11	7.15E-01	1.58E+11	1.12E+00	2.41E+09
3.00E-02	2.24E+11	4.01E-01	2.63E+11	7.16E-01	3.60E+08	1.12E+00	2.09E+08
3.17E-02	2.56E+11	4.02E-01	3.60E+08	7.23E-01	5.03E+10	1.13E+00	2.75E+08
3.19E-02	1.06E+10	4.44E-01	1.09E+11	7.24E-01	3.81E+10	1.13E+00	6.07E+08
3.57E-02	5.73E+11	4.45E-01	1.06E+09	7.50E-01	1.87E+11	1.14E+00	3.36E+08
3.59E-02	2.46E+10	4.50E-01	1.30E+10	7.56E-01	2.18E+09	1.14E+00	4.55E+08
4.50E-02	1.37E+12	4.75E-01	1.80E+11	7.57E-01	8.61E+09	1.17E+00	7.93E+08
4.53E-02	1.31E+09	4.76E-01	4.74E+09	7.95E-01	1.38E+10	1.17E+00	5.84E+09
6.00E-02	8.36E+11	4.78E-01	1.44E+10	7.96E-01	2.77E+11	1.17E+00	1.53E+08
6.02E-02	1.17E+09	4.79E-01	4.17E+08	7.56E-01	1.82E+09	1.17E+00	2.98E+10
6.80E-02	4.43E+11	5.57E-01	5.60E+11	7.57E-01	2.83E+10	1.24E+00	2.04E+09

Energy (MeV)	Photon Source Strength (γ/s)	Energy (MeV)	Photon Source Strength (γ /s)	Energy (MeV)	Photon Source Strength (γ /s)	Energy (MeV)	Photon Source Strength (γ /s)
1.24E+00	2.46E+08	1.33E+00	2.98E+10	1.50E+00	1.53E+08	3.00E+00	3.57E+07
1.25E+00	1.22E+08	1.37E+00	9.76E+08	1.60E+00	9.35E+08	4.00E+00	3.33E+06
1.25E+00	1.63E+09	1.37E+00	9.87E+09	1.60E+00	3.39E+09	6.00E+00	2.52E+03
1.27E+00	8.24E+08	1.49E+00	3.91E+09	2.00E+00	3.93E+09	8.00E+00	2.89E+02
1.28E+00	6.64E+10	1.50E+00	1.33E+09	2.50E+00	6.79E+08	1.10E+01	3.31E+01
1.33E+00	1.74E+09						

Table XXI: Neutron energy group and respective source strength.

Energy (MeV)	Neutron Source Strength (n/s)	Energy (MeV)	Neutron Source Strength (n/s)	Energy (MeV)	Neutron Source Strength (n/s)	Energy (MeV)	Neutron Source Strength (n/s)
0.00E+00	0.00E+00	5.04E-06	7.52E-05	1.06E-02	4.68E+00	2.13E-01	1.36E+02
5.00E-10	1.89E-09	6.48E-06	1.08E-04	1.17E-02	3.76E+00	2.24E-01	1.46E+02
2.00E-09	2.95E-09	8.32E-06	1.57E-04	1.50E-02	1.23E+01	2.35E-01	1.56E+02
5.00E-09	5.39E-09	1.07E-05	2.26E-04	1.93E-02	1.79E+01	2.47E-01	1.67E+02
1.00E-08	1.22E-08	1.37E-05	3.28E-04	2.19E-02	1.18E+01	2.73E-01	3.69E+02
1.45E-08	1.43E-08	1.76E-05	4.74E-04	2.36E-02	8.20E+00	2.87E-01	2.04E+02
2.10E-08	2.51E-08	2.26E-05	6.87E-04	2.42E-02	2.95E+00	2.95E-01	1.07E+02
3.00E-08	4.19E-08	2.90E-05	9.97E-04	2.48E-02	3.06E+00	2.97E-01	3.99E+01
4.00E-08	5.48E-08	3.73E-05	1.45E-03	2.61E-02	6.48E+00	2.99E-01	1.90E+01
5.00E-08	6.22E-08	4.79E-05	2.19E-03	2.70E-02	4.90E+00	3.02E-01	5.18E+01
7.00E-08	1.44E-07	6.14E-05	3.29E-03	2.85E-02	7.97E+00	3.34E-01	4.82E+02
1.00E-07	2.57E-07	7.89E-05	4.76E-03	3.18E-02	1.84E+01	3.69E-01	5.48E+02
1.25E-07	2.47E-07	1.01E-04	6.89E-03	3.43E-02	1.44E+01	3.88E-01	3.02E+02
1.50E-07	2.73E-07	1.30E-04	1.00E-02	4.09E-02	4.03E+01	4.08E-01	3.23E+02
1.84E-07	5.54E-07	1.67E-04	1.45E-02	4.63E-02	3.59E+01	4.51E-01	7.11E+02
2.25E-07	7.42E-07	2.15E-04	2.09E-02	5.25E-02	4.31E+01	4.98E-01	8.04E+02
2.75E-07	9.76E-07	2.75E-04	3.03E-02	5.66E-02	2.99E+01	5.23E-01	4.40E+02
3.25E-07	1.05E-06	3.54E-04	4.43E-02	6.74E-02	8.38E+01	5.50E-01	4.66E+02
3.67E-07	9.25E-07	4.54E-04	6.42E-02	7.20E-02	3.78E+01	5.78E-01	4.94E+02
4.14E-07	1.10E-06	5.83E-04	9.26E-02	7.95E-02	6.38E+01	6.08E-01	5.23E+02
5.00E-07	2.13E-06	7.49E-04	1.35E-01	8.25E-02	2.63E+01	6.39E-01	5.53E+02
5.32E-07	8.21E-07	9.61E-04	1.96E-01	8.65E-02	3.59E+01	6.72E-01	5.84E+02
6.25E-07	2.55E-06	1.23E-03	2.87E-01	9.80E-02	1.07E+02	7.07E-01	6.17E+02

Energy (MeV)	Neutron Source Strength (n/s)	Energy (MeV)	Neutron Source Strength (n/s)	Energy (MeV)	Neutron Source Strength (n/s)	Energy (MeV)	Neutron Source Strength (n/s)
6.83E-07	1.65E-06	1.23E-01	6.27E+01	1.74E+00	1.43E+03	6.59E+00	1.40E+02
8.00E-07	3.55E-06	1.29E-01	6.75E+01	1.83E+00	1.49E+03	6.70E+00	6.30E+01
8.76E-07	2.43E-06	1.36E-01	7.26E+01	1.92E+00	1.57E+03	7.05E+00	1.64E+02
1.00E-06	4.13E-06	1.43E-01	7.78E+01	2.02E+00	1.63E+03	7.41E+00	1.31E+02
1.04E-06	1.39E-06	1.50E-01	8.37E+01	2.12E+00	1.69E+03	7.79E+00	1.03E+02
1.08E-06	1.41E-06	1.58E-01	8.98E+01	2.23E+00	1.76E+03	8.19E+00	7.95E+01
1.13E-06	1.62E-06	1.66E-01	9.65E+01	2.31E+00	1.21E+03	8.61E+00	6.01E+01
1.30E-06	6.52E-06	1.74E-01	1.03E+02	2.35E+00	6.10E+02	9.05E+00	4.46E+01
1.45E-06	5.71E-06	1.83E-01	1.11E+02	2.37E+00	3.07E+02	9.51E+00	3.23E+01
1.86E-06	1.75E-05	1.93E-01	1.19E+02	2.39E+00	3.10E+02	1.00E+01	2.30E+01
2.38E-06	2.52E-05	2.02E-01	1.27E+02	2.47E+00	1.24E+03	1.05E+01	1.59E+01
3.06E-06	3.62E-05	7.43E-01	6.53E+02	2.59E+00	1.87E+03	1.11E+01	1.08E+01
3.93E-06	5.21E-05	7.81E-01	6.89E+02	2.73E+00	1.86E+03	1.16E+01	7.08E+00
1.59E-03	4.20E-01	8.21E-01	7.25E+02	2.87E+00	1.83E+03	1.22E+01	4.55E+00
2.04E-03	6.07E-01	8.63E-01	7.64E+02	3.01E+00	1.75E+03	1.25E+01	1.59E+00
2.25E-03	3.13E-01	9.07E-01	8.03E+02	3.17E+00	1.65E+03	1.28E+01	1.24E+00
2.49E-03	3.64E-01	9.62E-01	9.87E+02	3.33E+00	1.54E+03	1.35E+01	1.71E+00
2.61E-03	2.03E-01	1.00E+00	7.43E+02	3.68E+00	2.64E+03	1.38E+01	5.69E-01
2.75E-03	2.19E-01	1.11E+00	1.90E+03	4.07E+00	2.02E+03	1.42E+01	4.33E-01
3.04E-03	4.93E-01	1.17E+00	1.02E+03	4.49E+00	1.48E+03	1.46E+01	3.25E-01
3.36E-03	5.72E-01	1.23E+00	1.07E+03	4.72E+00	6.02E+02	1.49E+01	2.42E-01
3.71E-03	6.63E-01	1.29E+00	1.12E+03	4.97E+00	5.34E+02	1.57E+01	3.10E-01
4.31E-03	1.21E+00	1.35E+00	1.16E+03	5.22E+00	4.70E+02	1.65E+01	1.63E-01
5.53E-03	2.73E+00	1.42E+00	1.21E+03	5.49E+00	4.07E+02	1.69E+01	4.86E-02
7.10E-03	3.98E+00	1.50E+00	1.27E+03	5.77E+00	3.48E+02	1.73E+01	3.41E-02
9.12E-03	5.78E+00	1.57E+00	1.32E+03	6.07E+00	2.94E+02	1.96E+01	6.39E-02
1.11E-01	1.29E+02	1.65E+00	1.38E+03	6.38E+00	2.46E+02	2.00E+01	2.53E-03
1.17E-01	5.84E+01						

APPENDIX B

CANDU Fuel Material Composition

Natural Uranium		**Grams/tU**	
^{234}U		55.0	
^{235}U		7115.0	
^{238}U		992830.0	
Impurities in CANDU Fuel Material			
Elements	**Grams/tU**	**Elements**	**Grams/tU**
Oxygen	134454.0	Vanadium	3.0
Lithium	1.0	Chromium	4.0
Boron	1.0	Manganese	1.7
Carbon	86.4	Iron	18.0
Nitrogen	25.0	Cobalt	1.0
Fluorine	10.7	Nickel	24.0
Sodium	15.0	Copper	1.0
Magnesium	2.0	Zinc	40.3
Aluminium	16.7	Molybdenum	10.0
Silicon	12.1	Silver	0.1
Phosphorus	35.0	Cadmium	25.0
Chlorine	5.3	Indium	2.0
Calcium	2.0	Tin	4.0
Titanium	1.0	Gadolinium	2.5
Lead	1.0	Tungsten	2.0
Bismuth	0.4		

APPENDIX C

Cladding (Zircaloy-4) Material Composition

Elements	**Grams/kg**	**Elements**	**Grams/kg**
Zirconium	979.11	Hafnium	0.078
Tin	16	Hydrogen	0.013
Iron	2.25	Manganese	0.02
Chromium	1.25	Nitrogen	0.08
Nickel	0.02	Oxygen	0.95
Aluminium	0.024	Sulfur	0.035
Boron	0.00033	Titanium	0.02
Cadmium	0.00025	Tungsten	0.02
Carbon	0.12	Vanadium	0.02
Cobalt	0.01	Uranium	0.0002
Copper	0.02		

APPENDIX D

MCNP input of a CANDU6 Fuel bundle

```
CANDU6 37 Element Fuel Bundle
    1     1 -10.1154 -2   4 -5      $ fuel pellet
    2     2 -6.55     2  -3  4 -5   $ clad
    3     1 -10.1154 -8   4 -5      $ fuel pellet
    4     2 -6.55     8  -9  4 -5   $ clad
    5     1 -10.1154 -11  4 -5      $ fuel pellet
    6     2 -6.55     11 -12 4 -5   $ clad
    7     1 -10.1154 -14  4 -5      $ fuel pellet
    8     2 -6.55     14 -15 4 -5   $ clad
    9     1 -10.1154 -17  4 -5      $ fuel pellet
   10     2 -6.55     17 -18 4 -5   $ clad
   11     1 -10.1154 -20  4 -5      $ fuel pellet
   12     2 -6.55     20 -21 4 -5   $ clad
   13     1 -10.1154 -23  4 -5      $ fuel pellet
   14     2 -6.55     23 -24 4 -5   $ clad
   15     1 -10.1154 -26  4 -5      $ fuel pellet
   16     2 -6.55     26 -27 4 -5   $ clad
   17     1 -10.1154 -29  4 -5      $ fuel pellet
   18     2 -6.55     29 -30 4 -5   $ clad
   19     1 -10.1154 -32  4 -5      $ fuel pellet
   20     2 -6.55     32 -33 4 -5   $ clad
   21     1 -10.1154 -35  4 -5      $ fuel pellet
   22     2 -6.55     35 -36 4 -5   $ clad
   23     1 -10.1154 -38  4 -5      $ fuel pellet
   24     2 -6.55     38 -39 4 -5   $ clad
   25     1 -10.1154 -41  4 -5      $ fuel pellet
   26     2 -6.55     41 -42 4 -5   $ clad
   27     1 -10.1154 -44  4 -5      $ fuel pellet
   28     2 -6.55 44 -45  4 -5      $ clad
   29     1 -10.1154 -47  4 -5      $ fuel pellet
   30     2 -6.55 47 -48  4 -5      $ clad
   31     1 -10.1154 -50  4 -5      $ fuel pellet
   32     2 -6.55     50 -51 4 -5   $ clad
   33     1 -10.1154 -53  4 -5      $ fuel pellet
   34     2 -6.55     53 -54 4 -5   $ clad
   35     1 -10.1154 -56  4 -5      $ fuel pellet
   36     2 -6.55     56 -57 4 -5   $ clad
   37     1 -10.1154 -59  4 -5      $ fuel pellet
   38     2 -6.55     59 -60 4 -5   $ clad
   39     1 -10.1154 -62  4 -5      $ fuel pellet
   40     2 -6.55 62 -63  4 -5      $ clad
   41     1 -10.1154 -65  4 -5      $ fuel pellet
   42     2 -6.55     65 -66 4 -5   $ clad
   43     1 -10.1154 -68  4 -5      $ fuel pellet
```

```
   44     2 -6.55     68 -69  4 -5  $ clad
   45     1 -10.1154 -71  4  -5     $ fuel pellet
   46     2 -6.55     71 -72  4 -5  $ clad
   47     1 -10.1154 -74  4  -5     $ fuel pellet
   48     2 -6.55 74 -75  4  -5     $ clad
   49     1 -10.1154 -77  4  -5     $ fuel pellet
   50     2 -6.55     77 -78  4 -5  $ clad
   51     1 -10.1154 -80  4  -5     $ fuel pellet
   52     2 -6.55     80 -81  4 -5  $ clad
   53     1 -10.1154 -83  4  -5     $ fuel pellet
   54     2 -6.55     83 -84  4 -5  $ clad
   55     1 -10.1154 -86  4  -5     $ fuel pellet
   56     2 -6.55     86 -87  4 -5  $ clad
   57     1 -10.1154 -89  4  -5     $ fuel pellet
   58     2 -6.55     89 -90  4 -5  $ clad
   59     1 -10.1154 -92  4  -5     $ fuel pellet
   60     2 -6.55     92 -93  4 -5  $ clad
   61     1 -10.1154 -95  4  -5     $ fuel pellet
   62     2 -6.55     95 -96  4 -5  $ clad
   63     1 -10.1154 -98  4  -5     $ fuel pellet
   64     2 -6.55     98 -99  4 -5  $ clad
   65     1 -10.1154 -101 4  -5     $ fuel pellet
   66     2 -6.55     101 -102 4 -5 $ clad
   67     1 -10.1154 -104  4  -5    $ fuel pellet
   68     2 -6.55     104 -105 4 -5 $ clad
   69     1 -10.1154 -107  4  -5    $ fuel pellet
   70     2 -6.55     107 -108 4 -5 $ clad
   71     1 -10.1154 -110  4  -5    $ fuel pellet
   72     2 -6.55     110 -111 4 -5 $ clad
   73     1 -10.1154 -113  4  -5    $ fuel pellet
   74     2 -6.55     113 -114 4 -5 $ clad
   75     0 3 9 12 15 18 21 24 27 30 33 $ outside fuel pins
          36 39 42 45 48 51 54 57 60 63 66 69 72 75 78 81
          84 87 90 93 96 99 102 105 108 111 114 (-6 4 -5)
c HPGe modeling starts
  201     0         -201            $ void inside Ge
  202     3   -5.32  201 -202       $ Ge
  203     4  -0.535  202 -203       $ Li (0.5mm)
  204     0          203 -204 #206  $ 5mm gap
  205     5    -2.7  204 -205       $ Al
  206     5    -2.7 -206  207 -208  $ Al cap for detector
c empty space after fuel bundle; HPGe location)
  207     0    6 -209 4 -5 #201 #202 #203 #204 #205 #206
  208     0        209:-4 :5        $ outside world

    1        cz 0.6075             $ fuel outer
    2        cz 0.61175            $ clad air gap outer
    3        cz 0.65375            $ clad outer
    4        pz -24.75             $ fuel pin bottom
```

```
     5        pz 24.75               $ fuel pin top
     6        cz 12
c 1st ring radius 1.4885 (6 pins)
     7       c/z  1.4885  0 0.6075
     8       c/z  1.4885  0 0.61175
     9       c/z  1.4885  0 0.65375
    10       c/z -1.4885  0 0.6075
    11       c/z -1.4885  0 0.61175
    12       c/z -1.4885  0 0.65375
    13       c/z  0.74425 1.289079 0.6075
    14       c/z  0.74425 1.289079 0.61175
    15       c/z  0.74425 1.289079 0.65375
    16       c/z -0.74425 1.289079 0.6075
    17       c/z -0.74425 1.289079 0.61175
    18       c/z -0.74425 1.289079 0.65375
    19       c/z  0.74425 -1.289079 0.6075
    20       c/z  0.74425 -1.289079 0.61175
    21       c/z  0.74425 -1.289079 0.65375
    22       c/z -0.74425 -1.289079 0.6075
    23       c/z -0.74425 -1.289079 0.61175
    24       c/z -0.74425 -1.289079 0.65375
c 2nd ring radius 2.8755 (12 pins)
    25       c/z  2.77579 0.74425 0.6075
    26       c/z  2.77579 0.74425 0.61175
    27       c/z  2.77579 0.74425 0.65375
    28       c/z  2.77579 -0.74425 0.6075
    29       c/z  2.77579 -0.74425 0.61175
    30       c/z  2.77579 -0.74425 0.65375
    31       c/z -2.77579 0.74425 0.6075
    32       c/z -2.77579 0.74425 0.61175
    33       c/z -2.77579 0.74425 0.65375
    34       c/z -2.77579 -0.74425 0.6075
    35       c/z -2.77579 -0.74425 0.61175
    36       c/z -2.77579 -0.74425 0.65375
    37       c/z  0.74425 2.777579 0.6075
    38       c/z  0.74425 2.777579 0.61175
    39       c/z  0.74425 2.777579 0.65375
    40       c/z  0.74425 -2.777579 0.6075
    41       c/z  0.74425 -2.777579 0.61175
    42       c/z  0.74425 -2.777579 0.65375
    43       c/z -0.74425 2.777579 0.6075
    44       c/z -0.74425 2.777579 0.61175
    45       c/z -0.74425 2.777579 0.65375
    46       c/z -0.74425 -2.777579 0.6075
    47       c/z -0.74425 -2.777579 0.61175
    48       c/z -0.74425 -2.777579 0.65375
    49       c/z  2.033329 1.933618 0.6075
    50       c/z  2.033329 1.933618 0.61175
    51       c/z  2.033329 1.933618 0.65375
```

```
    52       c/z -2.033329 1.933618 0.6075
    53       c/z -2.033329 1.933618 0.61175
    54       c/z -2.033329 1.933618 0.65375
    55       c/z  2.033329 -1.933618 0.6075
    56       c/z  2.033329 -1.933618 0.61175
    57       c/z  2.033329 -1.933618 0.65375
    58       c/z -2.033329 -1.933618 0.6075
    59       c/z -2.033329 -1.933618 0.61175
    60       c/z -2.033329 -1.933618 0.65375
c 3rd ring radius 4.3305 (18 pins)
    61       c/z  0.74425 4.266079 0.6075
    62       c/z  0.74425 4.266079 0.61175
    63       c/z  0.74425 4.266079 0.65375
    64       c/z  0.74425 -4.266079 0.6075
    65       c/z  0.74425 -4.266079 0.61175
    66       c/z  0.74425 -4.266079 0.65375
    67       c/z -0.74425 4.266079 0.6075
    68       c/z -0.74425 4.266079 0.61175
    69       c/z -0.74425 4.266079 0.65375
    70       c/z -0.74425 -4.266079 0.6075
    71       c/z -0.74425 -4.266079 0.61175
    72       c/z -0.74425 -4.266079 0.65375
    73       c/z  4.3305 0 0.6075
    74       c/z  4.3305 0 0.61175
    75       c/z  4.3305 0 0.65375
    76       c/z -4.3305 0 0.6075
    77       c/z -4.3305 0 0.61175
    78       c/z -4.3305 0 0.65375
    79       c/z  2.16525 3.750323 0.6075
    80       c/z  2.16525 3.750323 0.61175
    81       c/z  2.16525 3.750323 0.65375
    82       c/z -2.16525 3.750323 0.6075
    83       c/z -2.16525 3.750323 0.61175
    84       c/z -2.16525 3.750323 0.65375
    85       c/z  2.16525 -3.750323 0.6075
    86       c/z  2.16525 -3.750323 0.61175
    87       c/z  2.16525 -3.750323 0.65375
    88       c/z -2.16525 -3.750323 0.6075
    89       c/z -2.16525 -3.750323 0.61175
    90       c/z -2.16525 -3.750323 0.65375
    91       c/z  4.066658 1.4885 0.6075
    92       c/z  4.066658 1.4885 0.61175
    93       c/z  4.066658 1.4885 0.65375
    94       c/z  4.066658 -1.4885 0.6075
    95       c/z  4.066658 -1.4885 0.61175
    96       c/z  4.066658 -1.4885 0.65375
    97       c/z -4.066658 1.4885 0.6075
    98       c/z -4.066658 1.4885 0.61175
    99       c/z -4.066658 1.4885 0.65375
```

```
  100       c/z -4.066658 -1.4885 0.6075
  101       c/z -4.066658 -1.4885 0.61175
  102       c/z -4.066658 -1.4885 0.65375
  103       c/z  3.32142 2.78923 0.6075
  104       c/z  3.32142 2.78923 0.61175
  105       c/z  3.32142 2.78923 0.65375
  106       c/z  3.32142 -2.78923 0.6075
  107       c/z  3.32142 -2.78923 0.61175
  108       c/z  3.32142 -2.78923 0.65375
  109       c/z -3.32142 2.78923 0.6075
  110       c/z -3.32142 2.78923 0.61175
  111       c/z -3.32142 2.78923 0.65375
  112       c/z -3.32142 -2.78923 0.6075
  113       c/z -3.32142 -2.78923 0.61175
  114       c/z -3.32142 -2.78923 0.65375
c HPGe surfaces
  201       rcc -20 0 0 2.38125 0 0 0.68
  202       rcc -20 0 0 6.15 0 0 3.25
  203       rcc -20 0 0 6.2 0 0 3.3
  204       rcc -20 0 0 6.7 0 0 3.8
  205       rcc -20 0 0 6.85 0 0 3.95
  206        cx  3.3
  207        px -13.7
  208        px -13.6
  209        cz  100

mode p
sdef pos=d1 rad=d2 axs=0 0 1 ext=d3 erg=d4
si1 L  0         0          0
       1.4885    0          0
      -1.4885    0          0
       0.74425   1.289079   0
      -0.74425   1.289079   0
       0.74425  -1.289079   0
      -0.74425  -1.289079   0
       2.77579   0.74425    0
       2.77579  -0.74425    0
      -2.77579   0.74425    0
      -2.77579  -0.74425    0
       0.74425   2.777579   0
       0.74425  -2.777579   0
      -0.74425   2.777579   0
      -0.74425  -2.777579   0
       2.033329  1.933618   0
      -2.033329  1.933618   0
       2.033329 -1.933618   0
      -2.033329 -1.933618   0
       0.74425   4.266079   0
       0.74425  -4.266079   0
```

```
      -0.74425   4.266079   0
      -0.74425  -4.266079   0
       4.3305    0          0
      -4.3305    0          0
       2.16525   3.750323   0
      -2.16525   3.750323   0
       2.16525  -3.750323   0
      -2.16525  -3.750323   0
       4.066658  1.4885     0
       4.066658 -1.4885     0
      -4.066658  1.4885     0
      -4.066658 -1.4885     0
       3.32142   2.78923    0
       3.32142  -2.78923    0
      -3.32142   2.78923    0
      -3.32142  -2.78923    0
sp1 D 1 36r
si2 0 0.65375
sp2 -21 1
si3 -24.75 24.75
sp3 0 1
si4 H 0.0000E+00  9.0000E-04   9.2000E-04   7.0000E-03
      7.2000E-03  8.5000E-03   8.7000E-03   9.2000E-03
      9.4000E-03  1.0200E-02   1.0600E-02   1.1000E-02
      1.1400E-02  2.0000E-02   2.6400E-02   2.6600E-02
      2.7400E-02  2.7600E-02   2.8600E-02   2.8800E-02
      3.0000E-02  3.1700E-02   3.1900E-02   3.5700E-02
      3.5900E-02  4.5000E-02   4.5300E-02   6.0000E-02
      6.0200E-02  6.8000E-02   6.8200E-02   7.0000E-02
      8.6000E-02  8.6200E-02   8.6500E-02   8.6700E-02
      1.0000E-01  1.0100E-01   1.0500E-01   1.0600E-01
      1.2300E-01  1.2400E-01   1.2700E-01   1.2800E-01
      1.5000E-01  1.8800E-01   1.8900E-01   2.4700E-01
      2.4800E-01  3.0000E-01   4.0100E-01   4.0200E-01
      4.4400E-01  4.4500E-01   4.5000E-01   4.7500E-01
      4.7600E-01  4.7800E-01   4.7900E-01   5.5700E-01
      5.5800E-01  5.6300E-01   5.6400E-01   5.6900E-01
      5.7000E-01  5.8200E-01   5.8300E-01   5.9100E-01
      5.9200E-01  6.0400E-01   6.0500E-01   6.2500E-01
      6.2600E-01  6.6100E-01   6.6200E-01   6.7600E-01
      6.7700E-01  6.9200E-01   6.9300E-01   7.1500E-01
      7.1600E-01  7.2300E-01   7.2400E-01   7.5000E-01
      7.5600E-01  7.5700E-01   7.9500E-01   7.9600E-01
      8.0100E-01  8.0200E-01   8.1500E-01   8.1600E-01
      8.4500E-01  8.4600E-01   8.5000E-01   8.5100E-01
      8.7300E-01  8.7400E-01   8.9200E-01   8.9300E-01
      9.0400E-01  9.0500E-01   9.9600E-01   9.9700E-01
      1.0000E+00  1.0040E+00   1.0050E+00   1.0380E+00
      1.0390E+00  1.1180E+00   1.1190E+00   1.1280E+00
```

```
      1.1290E+00  1.1400E+00   1.1410E+00   1.1670E+00
      1.1680E+00  1.1730E+00   1.1740E+00   1.2410E+00
      1.2420E+00  1.2460E+00   1.2470E+00   1.2740E+00
      1.2750E+00  1.3320E+00   1.3330E+00   1.3650E+00
      1.3660E+00  1.4940E+00   1.4950E+00   1.5000E+00
      1.5960E+00  1.5970E+00   2.0000E+00   2.5000E+00
      3.0000E+00  4.0000E+00   6.0000E+00   8.0000E+00
      1.1000E+01
sp4 D 0.0000E+00  0.0000E+00  1.9938E+11  0.0000E+00
      1.2360E+10  0.0000E+00  5.6024E+11  0.0000E+00
      6.1565E+10  0.0000E+00  2.1944E+08  0.0000E+00
      5.9399E+09  8.0786E+12  1.9544E+12  6.2174E+08
      2.4430E+11  4.2622E+09  3.0538E+11  5.2094E+09
      3.6645E+11  2.7567E+11  2.6568E+10  6.1620E+11
      6.1565E+10  1.4756E+12  2.4870E+09  9.3203E+11
      2.2127E+09  4.9455E+11  1.7522E+11  1.1413E+11
      5.1311E+11  2.9258E+08  9.6208E+09  5.9980E+10
      4.2652E+11  1.2787E+11  3.2724E+10  3.9864E+10
      1.3908E+11  2.1785E+11  2.4543E+10  8.0252E+10
      1.7998E+11  2.2621E+11  1.1366E+09  3.4527E+11
      3.2724E+10  3.0955E+11  6.3163E+11  8.9980E+08
      2.6266E+11  2.6520E+09  3.1269E+10  2.3272E+11
      9.2258E+09  1.8618E+10  1.0419E+09  7.2610E+11
      1.2787E+09  4.6545E+10  5.2953E+10  4.6545E+10
      9.7502E+10  1.1171E+11  4.2148E+09  7.4471E+10
      2.3489E+10  1.1171E+11  6.1674E+11  1.8618E+11
      1.5154E+09  3.2581E+11  1.1980E+13  1.3032E+11
      7.5772E+08  1.3963E+11  8.4770E+09  2.0480E+11
      8.9980E+08  6.5162E+10  9.5237E+10  2.4203E+11
      2.5426E+09  2.1500E+10  1.6103E+10  5.3964E+11
      2.1188E+09  5.5165E+10  5.5090E+09  2.4152E+09
      1.2289E+10  2.7941E+09  1.6951E+09  1.1366E+09
      9.3229E+09  5.7777E+10  7.6278E+09  2.4152E+09
      4.6615E+09  4.2148E+09  3.8563E+10  4.9868E+10
      1.2713E+09  8.8768E+07  8.4818E+10  7.3234E+08
      6.3190E+09  1.7532E+09  5.2094E+08  1.9973E+08
      1.5154E+09  2.4411E+08  1.1366E+09  5.7699E+08
      1.1374E+10  1.1096E+08  3.7978E+12  1.4869E+09
      6.1565E+08  8.8768E+07  4.0728E+09  5.9919E+08
      1.6575E+11  1.2649E+09  3.7986E+12  7.1015E+08
      1.9210E+10  2.8406E+09  3.3150E+09  1.1096E+08
      3.0149E+08  8.4770E+09  1.2656E+09  1.1341E+09
      5.4861E+07  7.0688E+06  2.1946E+03  2.5133E+02
      2.8819E+01
m1    92000     -0.88148      $ UO2
      8016      -0.11852
m2    40000     -0.9817       $ Zirc-4
      50123     -0.01604
      26056     -0.00226
```

```
m3    32000     -1            $ Ge
m4    3000      -1            $ Li
m5    13000     -1            $ Al
imp:p             1 81r                  0
f8:p 202
ft8 GEB .0024 -.0014 -.6834
e8 0 1e-3 0.01 2747i 11.002
c fm8 4.4e+13
prdmp 1e8 1e8
nps 1e9
print
```

VITA

Name: Nandan Gowthahalli Chandregowda

Address: Texas A&M University, Department of Nuclear Engineering
337 Zachry Engineering Center
3133 TAMU
College Station, TX 77843-3133

Email Address: nandan1947@gmail.com

Education: B.S., Physics, Chemistry, Mathematics, Mangalore University, India, 2007
M.S., Radiation Physics, Mangalore University, India, 2009
M.S., Nuclear Engineering, Texas A&M University, 2012